Typhoon-Position-Oriented Sensitivity Analysis. Part I: Theory and Verification

KOSUKE ITO

Department of Atmospheric Sciences, National Taiwan University, Taipei, Taiwan, and Japan Agency for Marine-Earth Science and Technology, Yokohama, Japan

CHUN-CHIEH WU

Department of Atmospheric Sciences, National Taiwan University, Taipei, Taiwan

(Manuscript received 1 November 2012, in final form 2 February 2013)

ABSTRACT

A new sensitivity analysis method is proposed for the ensemble prediction system in which a tropical cyclone (TC) position is taken as a metric. Sensitivity is defined as a slope of linear regression (or its approximation) between state variable and a scalar representing the TC position based on ensemble simulation. The experiment results illustrate important regions for ensemble TC track forecast. The typhoon-position-oriented sensitivity analysis (TyPOS) is applied to Typhoon Shanshan (2006) for the verification time of up to 48 h. The sensitivity field of the TC central latitude with respect to the vorticity field obtained from large-scale random initial perturbation is characterized by a horizontally tilted pattern centered at the initial TC position. These sensitivity signals are generally maximized in the middle troposphere and are far more significant than those with respect to the divergence field. The results are consistent with the sensitivity signals obtained from existing methods. The verification experiments indicate that the signals from TyPOS quantitatively reflect an ensemble-mean position change as a response to the initial perturbation. Another experiment with Typhoon Dolphin (2008) demonstrates the long-term analysis of forecast sensitivity up to 96 h. Several additional tests have also been carried out to investigate the dependency among ensemble members, the impacts of using different horizontal grid spacing, and the effectiveness of ensemble-Kalman-filter-based perturbations.

1. Introduction

In terms of disaster prevention and mitigation associated with tropical cyclones (TCs), the accuracy of track forecasts is critical because forecasts of the intensity and the rainfall amount can result in large errors if the track forecast is inadequate (Wu and Kuo 1999; Chan 2010). During past decades, the physical processes governing the movement of TCs have been intensively investigated (Wu and Emanuel 1993; Elsberry 1995; Chan 2010). The 48-h track error has been almost halved owing to increased observations and many improvements in numerical weather prediction systems (National Hurricane Center 2012). However, ''busted'' cases in which track forecast errors exceed 1000 km in a 72-h forecast still occasionally occur (Yamaguchi et al. 2009, 2012; Japan Meteorological Agency 2010). Therefore, reducing track forecast errors remains one of the major issues for TC researchers and operational centers.

The errors in weather forecasts are mainly associated with two factors: imperfections of the numerical model and errors in the initial conditions (Yoden 2007). For a given model, additional observations from critical regions are supposed to reduce uncertainties in the initial conditions and lead to a better forecast. For the purpose of reducing errors in the track forecast, aircraft-borne observations have been ''targeted'' in the synoptic environment of TCs. At present, operational surveillance observations of TCs have been conducted by the National Oceanic and Atmospheric Administration (NOAA) in the Atlantic basin since 1997 (Aberson and Franklin 1999; Aberson 2003) and by the Dropwindsonde Observations for Typhoon Surveillance near the Taiwan Region (DOTSTAR) project (Wu et al. 2005) for selected western North Pacific TCs since 2003. In the summer of 2008, the issue of targeted observation was further explored in the Observing System Research and

Corresponding author address: Chun-Chieh Wu, Department of Atmospheric Sciences, National Taiwan University, 1, Sec. 4, Roosevelt Rd., Taipei 10617, Taiwan.
E-mail: cwu@typhoon.as.ntu.edu.tw

DOI: 10.1175/JAS-D-12-0301.1

Predictability Experiment (THORPEX) Pacific Asian Regional Campaign (T-PARC; Elsberry and Harr 2008; Weissmann et al. 2011; Chou et al. 2011; Wu et al. 2012a,b; Huang et al. 2012).

Several techniques for targeted observation guidance have been developed and compared to each other to identify ''sensitive'' regions (Majumdar et al. 2006; Reynolds et al. 2007; Wu et al. 2009a). These techniques include the total energy singular vector (SV) method used by the Navy Operational Global Atmospheric Prediction System (NOGAPS; Peng and Reynolds 2006; Chen et al. 2009), the European Centre for Medium-Range Weather Forecasts (ECMWF; Buizza et al. 2007), the Japan Meteorological Agency (JMA; Yamaguchi et al. 2009), and Yonsei University (YSU; Kim and Jung 2009; Kim et al. 2011); the adjoint-derived sensitivity steering vector (ADSSV) guidance (Wu et al. 2007, 2009b; Chen et al. 2011); the ensemble transform Kalman filter (ETKF; Majumdar et al. 2006, 2011); the analysis of ensemble deep-layer-mean (DLM) wind variance (Aberson 2003); and the conditional nonlinear optimal perturbation (CNOP) method (Mu et al. 2009). While TC track forecasts have been improved with additional observations in sensitive areas (e.g., Chou and Wu 2008; Yamaguchi et al. 2009; Chou et al. 2011), some differences can be found among different methods (Majumdar et al. 2006; Wu et al. 2009a). These differences stem from the different approaches to detect the sensitivity on TC motion as well as the different numerical models and configurations used (Wu et al. 2009b; Kim et al. 2011).

One potential way for further elaborating the sensitivity analysis method is to employ TC position as a metric, whereas existing methods use only TC steering flow (ADSSV) or total energy norms (SV, ETKF, and CNOP) at the verification time. The metrics employed in the existing studies are presumably relevant to TC motion, and several studies have shown that these methods can help capture the effect of synoptic features and binary interactions (e.g., Peng et al. 2007; Wu et al. 2007). Nevertheless, it is worth investigating a more direct evaluation of the sensitivity field on TC tracks by using TC position as a metric.

In this study, we propose a typhoon-position-oriented sensitivity analysis (TyPOS), which directly takes a TC position as a metric, for the ensemble prediction system. This technique is based on the ensemble-based sensitivity analysis method (Martin and Xue 2006; Ancell and Hakim 2007; Torn and Hakim 2008, 2009; Liu et al. 2008; Gombos and Hansen 2008; Sugiura 2010; Aonashi and Eito 2011). It has been applied to the sensitivity analysis of the minimum sea level pressure (SLP) and the root-mean-square error of SLP of TCs (Torn and Hakim 2009) as well as the 1000-hPa potential vorticity (Gombos et al. 2012). The ensemble-based sensitivity analysis has also been used to correct the displacement error suitable for real-world observations using the data assimilation technique (Aonashi and Eito 2011). These approaches motivate us to calculate the sensitivity field by employing TC position directly as a metric. Using this metric allows us to bypass the requirement of defining the metric associated with TC motion and to perform sensitivity analysis without constructing tangent linear and adjoint models.

In this study, we apply TyPOS to Typhoons Shanshan (2006) and Dolphin (2008). The synoptic sensitivity field affecting the TC motion is shown and verification tests are conducted to evaluate the response of the TC displacement to initial perturbations. This work is the first attempt to quantify the direction and distance of the TC vortex displacement directly by using the sensitivity field. A companion paper (hereafter referred to as Part II) will describe comparisons with other methods and provide physical interpretations of the sensitivity field in detail.

2. Theoretical background

a. Review of ensemble-based sensitivity

TyPOS is based on the ensemble-based sensitivity analysis recently developed by several researchers (Martin and Xue 2006; Ancell and Hakim 2007; Torn and Hakim 2008, 2009; Liu et al. 2008; Gombos and Hansen 2008; Sugiura 2010; Aonashi and Eito 2011). Here, we briefly outline this sensitivity analysis technique in a generalized manner.

Let $\mathbf{x}$ and j be an n degree-of-freedom input vector and output scalar, respectively. The input vector represents the perturbations in the physical variables at the initial time and the output scalar is a forecast metric. Considering m realizations of the input vector, $\mathbf{x}_i = (x_{1,i}, x_{2,i}, \ldots, x_{n,i})$, where $i(i = 1, 2, \ldots, m)$ represents the index of each ensemble member, with corresponding m realizations of j_i, we define matrix $\mathbf{X}$ and vector $\mathbf{j}$ as follows:

$$\mathbf{X} = \frac{1}{\sqrt{m-1}}(\delta\mathbf{x}_1, \delta\mathbf{x}_2, \ldots, \delta\mathbf{x}_m)^{\mathrm{T}}, \quad \text{and} \tag{1}$$

$$\mathbf{j} = \frac{1}{\sqrt{m-1}}(\delta j_1, \delta j_2, \ldots, \delta j_m)^{\mathrm{T}}. \tag{2}$$

Matrix $\mathbf{X}$ is composed of $\delta\mathbf{x}_i$ and the vector $\mathbf{j}$ is composed of δj_i, where δ indicates deviations from ensemble-mean values; that is, $\delta\mathbf{x}_i = \mathbf{x}_i - \langle\mathbf{x}\rangle$ and $\delta j_i = j_i - \langle j\rangle$. The angle brackets denote the ensemble mean and superscript T denotes the transpose. Note that the deviations are not necessarily infinitesimal, while Ancell and Hakim (2007) introduced the assumption $\partial J/\partial\mathbf{x} \approx \delta J/\delta\mathbf{x}$.

The generalized ensemble-based sensitivity is defined as follows (Gombos and Hansen 2008):

$$\boldsymbol{\lambda}_{\mathbf{x}}^{j} \equiv \mathbf{X}^{+}\mathbf{j}, \tag{3}$$

where the plus sign superscript indicates the Moore–Penrose generalized inverse matrix,[1] which can be computed from the equation below:

$$\mathbf{X}^{+} = \mathbf{V}\mathbf{D}^{+}\mathbf{U}^{\mathrm{T}}, \tag{4}$$

where $\mathbf{X} = \mathbf{U}\mathbf{D}^{+}\mathbf{V}^{\mathrm{T}}$ is the singular value decomposition of $\mathbf{X}$. The generalized inverse matrix $\mathbf{D}^{+}$ is formed by replacing every nonzero diagonal entry of $\mathbf{D}$ by its reciprocal and transpose the resulting matrix.

In this paper, the vector $\boldsymbol{\lambda}_{\mathbf{x}}^{j}$ is referred to as "sensitivity" and the kth component of $\boldsymbol{\lambda}_{\mathbf{x}}^{j}$ is denoted as $\lambda_{x_k}^{j}$ ($k = 1, 2, \ldots, n$). The reason why $\boldsymbol{\lambda}_{\mathbf{x}}^{j}$ is called the sensitivity is that it represents the generalized solution of inverse problem associated with a first-order relationship between $\mathbf{j}$ and $\mathbf{X}$,

$$\mathbf{j} = \mathbf{X}\hat{\boldsymbol{\lambda}}, \tag{5}$$

which means the vector $\hat{\boldsymbol{\lambda}}$ multiplied by initial perturbations in physical variables equals to perturbations in the forecast metric at the verification time.

If the number of ensemble members exceeds the degrees of freedom (i.e., $m > n$), a purely overdetermined problem, and the inverse of $(\mathbf{X}^{\mathrm{T}}\mathbf{X})^{-1}$ exists, the vector $\hat{\boldsymbol{\lambda}} = \boldsymbol{\lambda}_{\mathbf{x}}^{j}$ is the slope of regression line obtained from minimizing deviations as shown in Fig. 1 (Menke 1989). In other words, $\boldsymbol{\lambda}_{x_k}^{j}$ represents the ratio of changes in j to the change in x_k based on ensemble simulations. The vector $\boldsymbol{\lambda}_{\mathbf{x}}^{j}$ is the same as the adjoint sensitivity if the time evolution of initial perturbation is completely equivalent to that described by the tangent linear model and j is a continuous function of $\mathbf{x}$ (Ancell and Hakim 2007).

If the degrees of freedom of $\mathbf{x}$ exceeds the number of ensemble members (i.e., $m < n$), a purely underdetermined problem, the vector $\hat{\boldsymbol{\lambda}} = \boldsymbol{\lambda}_{\mathbf{x}}^{j}$ represents the solution that satisfies Eq. (5) and yields the minimum of $|\hat{\boldsymbol{\lambda}}|$ in the L_2 norm (Menke 1989). This type of solution is termed as a minimum length solution and is frequently used in tackling inverse problems. Although the vector $\boldsymbol{\lambda}_{\mathbf{x}}^{j}$ can still be interpreted as a slope with respect to $\mathbf{x}$ satisfying $\mathbf{j} = \mathbf{X}\hat{\boldsymbol{\lambda}}$, the additional condition (minimization of $|\hat{\boldsymbol{\lambda}}|$) is introduced to fully determine all the n elements of the sensitivity field from m realizations. Thus, we do not expect that this sensitivity would appropriately reflect the impact of changes in the input vector $\mathbf{x}$ on changes in the metric j when the number of ensemble members m is far smaller than the degrees of freedom of $\mathbf{x}$, which is n.

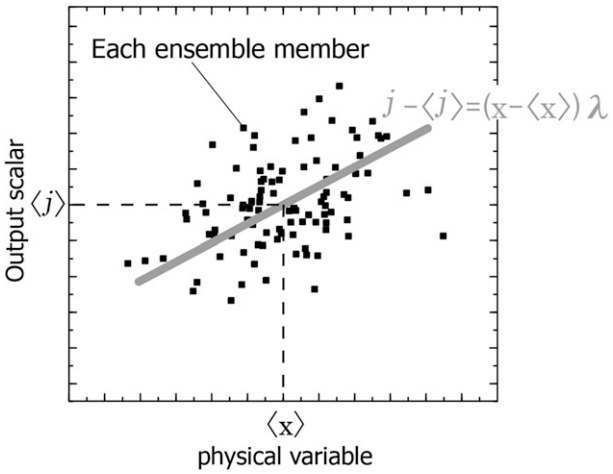

FIG. 1. Schematic illustration of the sensitivity with respect to a single degree of freedom. Angle brackets denote the ensemble-mean values.

If the inverse matrix of $\mathbf{X}^{\mathrm{T}}\mathbf{X}$ is known, the sensitivity can be obtained without executing the singular value decomposition in Eq. (4). By multiplying both sides of Eq. (5) by $\mathbf{X}^{\mathrm{T}}$, we obtain

$$\mathbf{X}^{\mathrm{T}}\mathbf{j} = \mathbf{X}^{\mathrm{T}}\mathbf{X}\hat{\boldsymbol{\lambda}}. \tag{6}$$

Since an element in the ath row and the bth column of $\mathbf{X}^{\mathrm{T}}\mathbf{X}$ is $[1/(m-1)]\sum_{i=1}^{m}\langle x_{a,i}x_{b,i}\rangle$, $\mathbf{X}^{\mathrm{T}}\mathbf{X}$ can be replaced by the ensemble covariance matrix. In particular, when the ensemble covariance matrix is diagonal, Eqs. (3) and (4) are reduced to the simplified equation below:

$$\lambda_{x_k}^{j} = \frac{\dfrac{1}{m-1}\displaystyle\sum_{i=1}^{m}\delta x_{k,i}\delta j_i}{\sigma_k^2}, \tag{7}$$

where σ_k^2 represents ensemble variance.[2]

b. TyPOS

TyPOS is an application of the ensemble-based sensitivity analysis designed for the ensemble forecast system.

[1] A Moore–Penrose generalized inverse matrix of $\mathbf{X}$ is defined as a matrix satisfying all of the following four criteria: (1) $\mathbf{X}\mathbf{X}^{+}\mathbf{X} = \mathbf{X}$, (2) $\mathbf{X}^{+}\mathbf{X}\mathbf{X}^{+} = \mathbf{X}$, (3) $(\mathbf{X}\mathbf{X}^{+})^{*} = \mathbf{X}\mathbf{X}^{+}$ and (4) $(\mathbf{X}^{+}\mathbf{X})^{*} = \mathbf{X}^{+}\mathbf{X}$, where the asterisk represents the adjoint matrix. The matrix exists and is unique. See more details in Menke (1989).

[2] Note that Eq. (7) is used as a definition of ensemble-based sensitivity for both diagonal and off-diagonal matrix in Ancell and Hakim (2007).

The input vector **x** represents perturbations in the physical variables at the initial time and the output scalar j is a scalar representing the vortex position such as longitude and latitude of the TC center at the verification time. TyPOS does not assume that the perturbations are infinitesimal. It fits our objective of employing TC position as a metric because it is not a differentiable function when reproduced in a dynamical model.

One problem is that the ensemble-based sensitivity is not expected to be a good indicator for sensitivity when the number of ensemble members is far smaller than the degrees of freedom of **x**. If we consider the sophisticated three-dimensional numerical model with n' degrees of freedom, it is not practical to perform simulations as much as n' times.

To resolve this problem, we consider a reduced-dimension space in which the n elements ($n < n'$) of x used for sensitivity analysis are sampled with larger grid spacing compared with that of the original numerical model in this work. The horizontal grid spacing can be greater than a few hundred kilometers if the aim is dealing with the synoptic features. In this work, the grid spacing used to define the sensitivity field differs from the grid spacing used to define the forecast metric. The grid points on the coarse mesh used for sensitivity calculation are referred to as the reduced grid points, while the grid points on the original model mesh used to perform the time integration are referred to as the model grid points. Here, initial perturbations in the reduced grid points are interpolated into the model grid points by cubic spline. The use of a basis function corresponding to the fast-developing modes is another option aside from employing the large-scale perturbations, which will be discussed in section 6b.

TyPOS has the potential to quantify the displacement distance and direction of ensemble-mean TC position. Suppose that the sensitivity approximates the ratio of changes in j to the change in x_k, ensemble-mean change in the output metric as a response to the initial perturbation is evaluated as follows (Δ denotes the perturbation relative to the control run):

$$\Delta\langle j\rangle \approx \sum \frac{1}{S}(\tilde{\lambda}^{j}_{x'}\Delta x'), \tag{8}$$

where Σ denotes the summation over all the model grid points and $\Delta x'$ represents the changes in the initial state defined at the model grid points. To complete the manipulation between the initial perturbations defined on model grid points and the sensitivity defined on reduced grid points, we introduce the interpolated sensitivity field defined on the model grid points $\tilde{\lambda}^{j}_{x'}$ and the scaling factor S. The scaling factor is defined as $S \equiv \|\tilde{\boldsymbol{\lambda}}\|/\|\boldsymbol{\lambda}\|$ (in L1 norm), which is based on the assumption that the influence of the initial changes in a reduced grid point is equivalent to the integrated influence of uniform initial condition changes in corresponding model grid points; that is, it has a large value when the reduced grid points are coarsely sampled from the model grid points. Equation (8) is useful for evaluating the magnitude of displacement as a response to changes in the initial state variables and for determining the priority of the targeted observations, although the expected displacement distance should be regarded as an approximation. This is due to the following reasons: the truncation error inherent in the projection, dependency on perturbation magnitudes, and the assumption that impacts are calculated by simple linear superposition of impacts from single grid points.

As stated in Torn and Hakim (2008), the reliability of sensitivity signals in TyPOS can be measured using a t test. The t test is relevant to the rejection of the null hypothesis that the slope of the output metric j with respect to the single variable x_k is zero (Wilks 2005). A higher confidence level is obtained with the increasing number of ensemble members or with statistically smaller deviations from the regression line if the values of the slope are equal. It is critical to distinguish meaningful signals from statistical noise, in particular, when the number of ensemble simulations is far smaller than the degrees of freedom of initial perturbations as demonstrated in section 6a.

c. *Summary of TyPOS*

Before applying the proposed method to a real-case calculation, the features and procedures are summarized here. In this methodology, TC position is taken as a forecast metric, and thus it is a direct method for a given ensemble prediction system. In addition to the clear objectivity, this method has several advantages. The method provides the possibility to evaluate the ensemble-mean vortex displacement direction and distance without using the tangent linear and adjoint models. To alleviate the burden posed by the enormous computational resources needed for obtaining the significant signals, we consider the reduced-dimension space and, if needed, to distinguish meaningful signals from noise using t tests.

The procedure of TyPOS is as follows: (i) generating m realizations with n degrees of freedom in the reduced grid points and projecting them onto the model variable space by cubic spline interpolation, (ii) performing the ensemble simulations m times after adding interpolated perturbation to the reference initial state, (iii) calculating the sensitivity by using the m realizations of the resultant metric that represents the TC position [Eqs. (3)

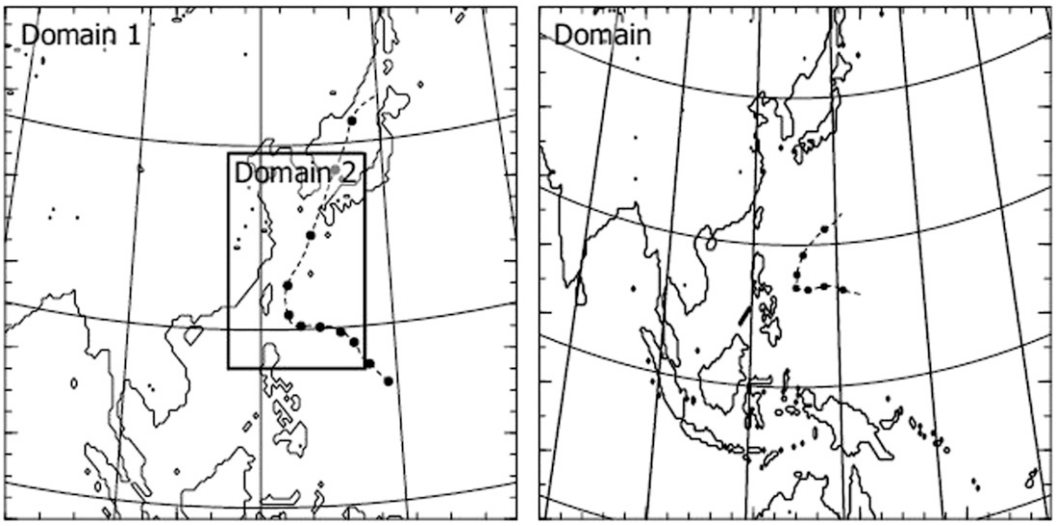

FIG. 2. The domains used in this experiment. (a) The dashed line indicates TC position from JMA best track for Typhoon Shanshan. Closed circles indicate TC positions at time intervals of 24 h from 0000 UTC 11 Sep. (b) As in (a), but for Typhoon Dolphin. Closed circles indicate the TC positions every 24 h from 0000 UTC 12 Dec 2008.

and (4), or Eq. (6)], (iv) (optional) evaluating the displacement of the vortex position by multiplying the changes in the initial state variable with the sensitivity field after the interpolation into the model grid points [Eq. (8)], and (v) (optional) conducting *t* tests to distinguish reliable signals from noise.

TyPOS can directly reflect the sensitivity field of the metric relevant to TC position for a given model and initial perturbations if the number of ensemble members is sufficiently large. However, TyPOS is still subject to a variety of uncertainties in terms of specifying initial perturbations. In this study, limitations arise from the

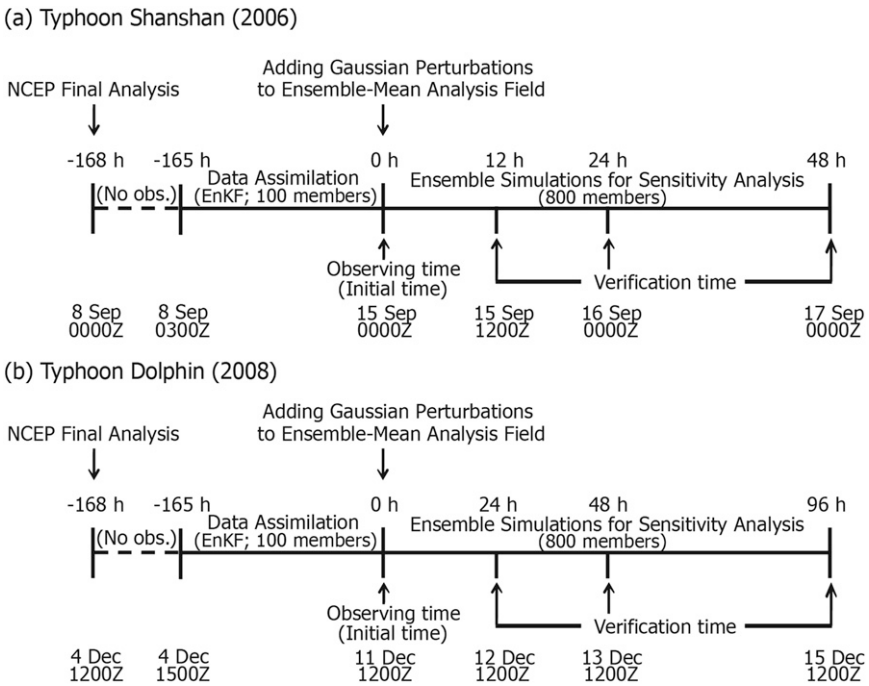

FIG. 3. Time schedule of the sensitivity analysis for (a) Typhoon Shanshan and (b) Typhoon Dolphin.

fact that dynamically balanced large-scale perturbations are employed as initial perturbations. A finescale feature is briefly discussed in section 6, although detailed examination is beyond the scope of this work.

Note that TyPOS is based on the linear regression obtained from ensemble simulation and the perturbation is not necessarily infinitesimal. Therefore, the validity of TyPOS is not limited to the time scale of tangent linear assumption as in any singular vector- or adjoint-based method. Nevertheless, care should be taken in interpreting the sensitivity, and the influence of nonlinear growth of perturbations requires further study.

3. Experimental design

a. Model configuration and time schedule

To assess the feasibility of TyPOS, we apply this method to Typhoon Shanshan, for which sensitivity analyses based on different targeted methods have already been conducted (Wu et al. 2009a,b; Reynolds et al. 2009; Chen et al. 2011), and Typhoon Dolphin, for which the spread of ensemble forecast TC track was reported to be large (from JMA 2009). The verification time is set to 12, 24, and 48 h for Shanshan in order to compare with the existing studies and to 24, 48, and 96 h for Dolphin in order to investigate its applicability to long-term sensitivity analyses with large uncertainties in track forecasts.

In this study, the Advanced Research Weather Research and Forecasting model (ARW-WRF), version 2.2.1 is employed to conduct the numerical simulation. The model configuration is the same as the doubly nested domain calculations of Wu et al. (2010). The coarse domain (domain 1) has 150 × 120 grid points (longitude by latitude) with the horizontal grid spacing of 54 km centered at 27.5°N, 120.0°E, while the fine-meshed domain (domain 2) has 120 × 150 grid points with the horizontal grid spacing of 18 km centered at 27.1°N, 124.9°E. The model contains 35 vertical levels in the terrain following sigma coordinate. The domains and TC positions from the JMA best track are shown in Fig. 2.

The prognostic state variables are perturbation of potential temperature, geopotential, and dry air mass in a column from the basic state as well as horizontal and vertical wind fields. Six mixing ratios (water vapor, cloud water, cloud ice, rain, snow, and graupel) are also forecast based on the WRF single-moment six-class graupel microphysics scheme (Hong et al. 2004; Hong and Lim 2006). Other parameterization schemes include the Rapid Radiative Transfer Model scheme (Mlawer et al. 1997) for longwave radiation, the simple shortwave scheme (Dudhia 1989) for shortwave radiation, and the YSU planetary boundary layer scheme (Hong et al. 2006). The Grell–Devenyi ensemble scheme (Grell and Devenyi 2002) is used for the parameterization of cumulus convection in both domains 1 and 2.

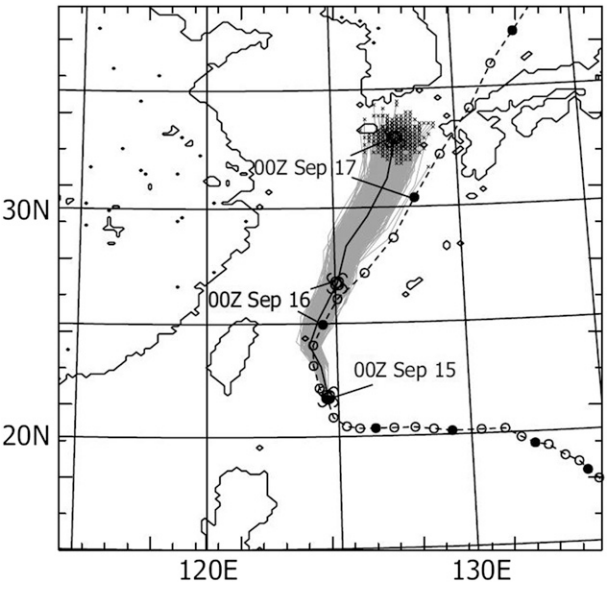

FIG. 4. The TC position from JMA best track for Typhoon Shanshan plotted over simulated tracks. Open circles indicate the TC positions every 6 h from 2100 UTC 10 Sep, while solid ones indicate the TC positions every 24 h from 0000 UTC 11 Sep. The TC symbols and thick solid lines indicate the ensemble-mean simulated track from 0000 UTC 15 Sep to 0000 UTC 17 Sep. The gray lines correspond to the tracks of each member. The large area of crosses near the top are the simulated positions of TC center at 0000 UTC 17 Sep.

To reproduce a realistic TC vortex, we performed a 1-week data assimilation with the ensemble Kalman filter (EnKF) technique prior to the sensitivity analysis. This data assimilation procedure starts from the field of National Centers for Environmental Prediction (NCEP) final analysis. The WRF-based EnKF data assimilation system used in this study is similar to the system in Meng and Zhang (2007, 2008a,b) and has been developed to adjust TC central position and pressure in order to fit the best track (Wu et al. 2010). In this study, the number of ensemble members in the EnKF system is 100. We regard 0000 UTC 15 September 2006 (1200 UTC 11 December 2008) as the initial time of the sensitivity analysis for Shanshan (Dolphin) and regard ensemble-mean state of the EnKF analysis field at this moment as the initial reference state. For simplicity, we assume that this initial time is the same as the observation time (i.e., no lead-time forecast experiment). For the presentation of results, the number of hours beginning from the initial time of the sensitivity analysis is used. The time schedule of the experiment is summarized in Fig. 3. In fact, we calculate the sensitivity both of latitude and longitude at the model grid point where the minimum pressure is

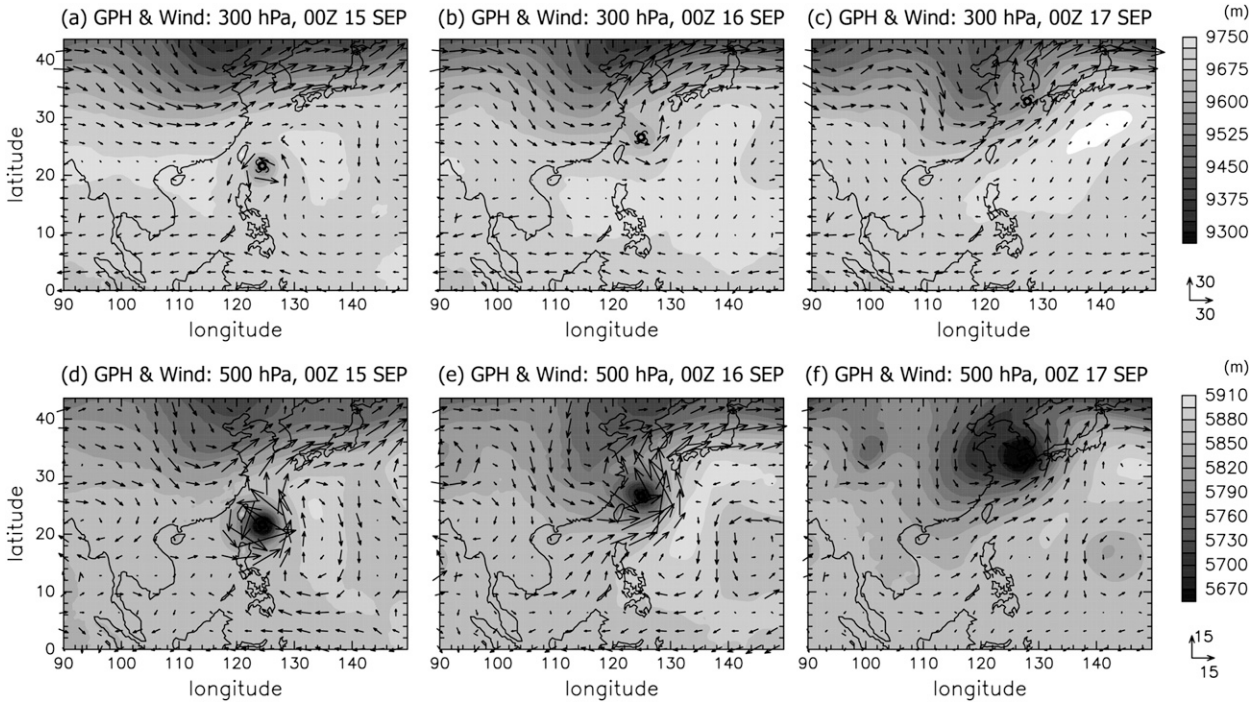

FIG. 5. Ensemble-mean geopotential height (shading) and horizontal wind (vectors) at (a)–(c) 300 and (d)–(f) 500 hPa based on 800 member forecasts at (a),(d) 0000 UTC 15 Sep, (b),(e) 0000 UTC 16 Sep, and (c),(f) 0000 UTC 17 Sep. Unit vectors for horizontal wind fields ($m\,s^{-1}$) are shown on the rhs of each row. The TC symbol indicates the ensemble-mean simulated position at each time.

achieved at the verification time. However, for concise presentation, we will present the only sensitivity of the latitude (longitude) for Shanshan (Dolphin) unless otherwise noted.

b. *Perturbations for sensitivity analysis*

To construct the sensitivity field, u and v at the initial time are perturbed. As a first step, the magnitude is simply determined so that the standard deviation becomes an uniform value of $1.8\,m\,s^{-1}$ ($1.4\,m\,s^{-1}$) for Shanshan (Dolphin), which is the same as the area-averaged spread of the 100 EnKF members in the middle troposphere at the initial time (figures not shown).

In this study, initial perturbations are generated independently in each reduced grid point and thus t tests are applied independently in each reduced grid point except in section 6b. The benefit of using the uncorrelated perturbations is that we can calculate the sensitivity based on the simplified Eq. (7). Independent Gaussian random numbers in each reduced grid point are generated by using the Mersenne twister method and Box–Mullar transform (Box and Muller 1958; Matsumoto and Nishimura 1998) and are added to the initial reference state of these variables. It is used to construct the sensitivity field with respect to u and v. Although the relative vorticity ζ and divergence ψ are not prognostic state variables in this model, these are essential variables for clear physical interpretation. Thus, the sensitivity field with respect to u and v is converted to one with respect to relative vorticity ζ and divergence ψ as in Kleist and Morgan (2005) and Wu et al. (2007).

The horizontal reduced grid spacing is set to 540 km regardless of the model grid spacing. This coarse grid spacing used in this study is presumably sufficient in resolving synoptic features of a few thousand kilometers, while not reflecting the finescale structures of the sensitivity field. The vertical grid points are sampled on $\sigma =$ 0.998 85, 0.8445, 0.5060, 0.2879, and 0.101. The potential temperature and geopotential fields are also changed so that the perturbation fields are close to geostrophic and hydrostatic balances as a response to initial perturbations of vorticity. For instance, the standard deviation of perturbations in potential temperature (geopotential) is 0.12 K ($30.1\,m^2\,s^{-2}$) at 20°N and $\sigma = 0.8445$ and 0.06 K ($14.2\,m^2\,s^{-2}$) at 20°N and $\sigma = 0.5060$ for Shanshan. To obtain temperature and geopotential perturbation fields, we follow the same procedure as in Komaromi et al. (2011). We first calculate the perturbation in streamfunction by solving Poisson's equation using a relaxation method and then calculate the temperature and geopotential perturbation field consistent with the streamfunction.

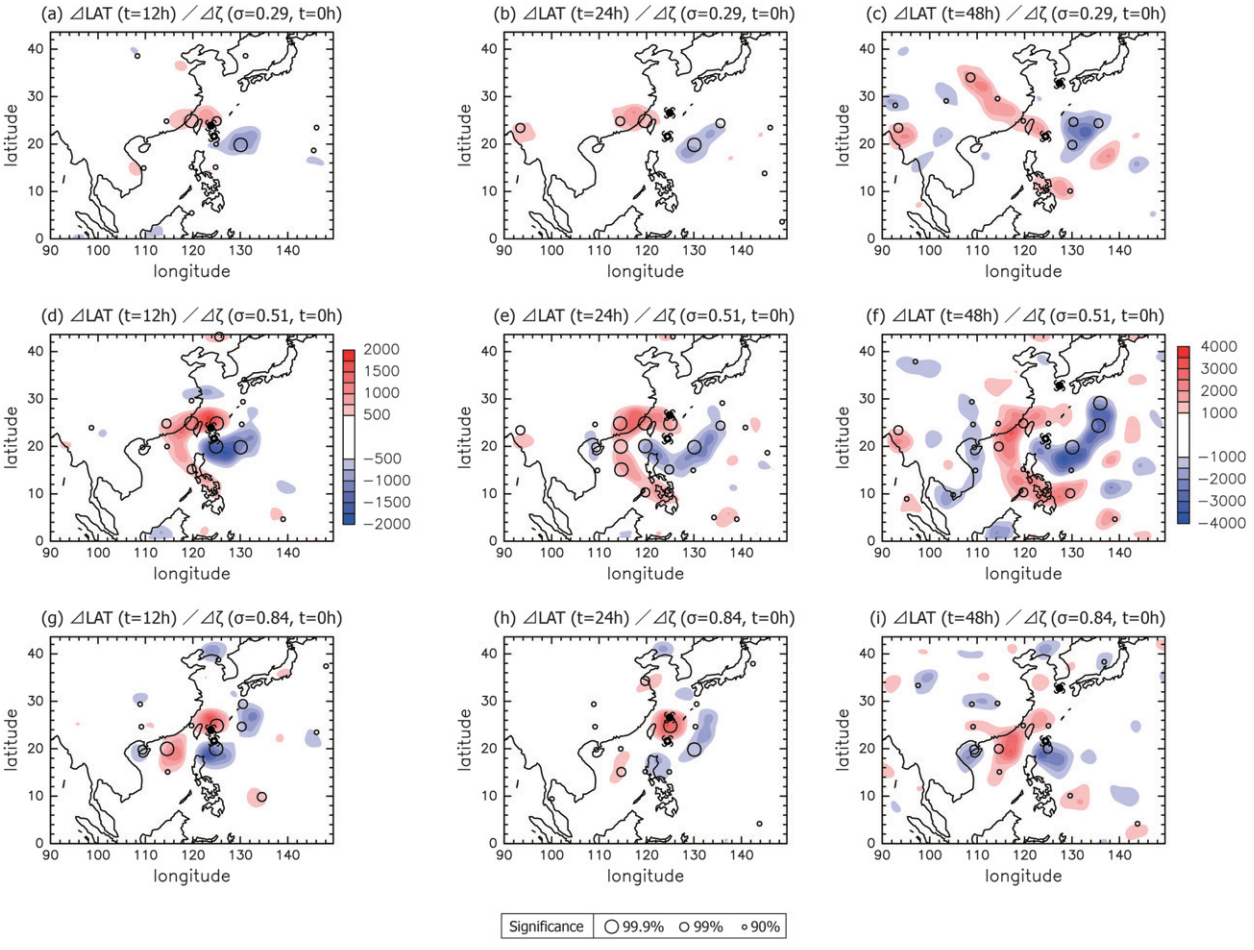

FIG. 6. Ensemble-based sensitivity of Typhoon Shanshan's central latitude with respect to the vorticity field (degree seconds): (left to right) $t = 12$, 24, and 48 h and (top to bottom) $\sigma = 0.29$, 0.51, and 0.84 at $t = 0$ h. The size of the circles in the panels indicates the results of significance t test at each reduced grid point: 99.9%, 99%, and 90%. The TC symbols with an open dot indicate the ensemble-mean TC positions at the initial time and closed TC symbols indicate those at the verification time. Left color bar indicates the values in the left column and right color bar indicates the values in the middle and right columns.

The number of ensemble simulations m is 800. However, 170 simulations for Dolphin are not used for sensitivity analysis because the maximum wind speed of the cyclone is reduced below the tropical storm intensity of 17.2 m s^{-1} during their lifetime. This threshold is introduced to strictly avoid false detection of TCs. The degrees of freedom of the initial perturbations n is 1800 for Shanshan ($15 \times 12 \times 5$ reduced grid points in the zonal, meridional, and vertical direction for the two components, u and v) and 3600 for Dolphin ($24 \times 15 \times 5 \times 2$). Therefore, the problems are formulated as underdetermined ones.

4. Sensitivity analysis for Shanshan

a. Synopsis and simulated track

Figure 4 shows the center position of Shanshan based on the JMA best track. It formed to the west of Guam and moved northwestward and started to recurve on 13 September, turning northward from its original westward path. The TC later began to accelerate northeastward on 16 September. During the period of the current numerical experiment, there are several synoptic features around the TC region. Figures 5a and 5d show that the location of Shanshan was between the midlatitude trough over northern–central China and the anticyclonic flow at the initial time (0000 UTC 15 September). On 16 September, Shanshan moved swiftly as it started to interact with a midlatitude trough over eastern China (Figs. 5b,e). On 17 September, Shanshan has become embedded in the midlatitude trough in the 500-hPa fields (Figs. 5c,f).

The simulated tracks of ensemble members from 0000 UTC 15 September to 0000 UTC 17 September are overlaid with TC symbols in Fig. 4. This shows that the TC central position is reproduced with a left-of-track bias. Ensemble spreads of the forecasted TC central

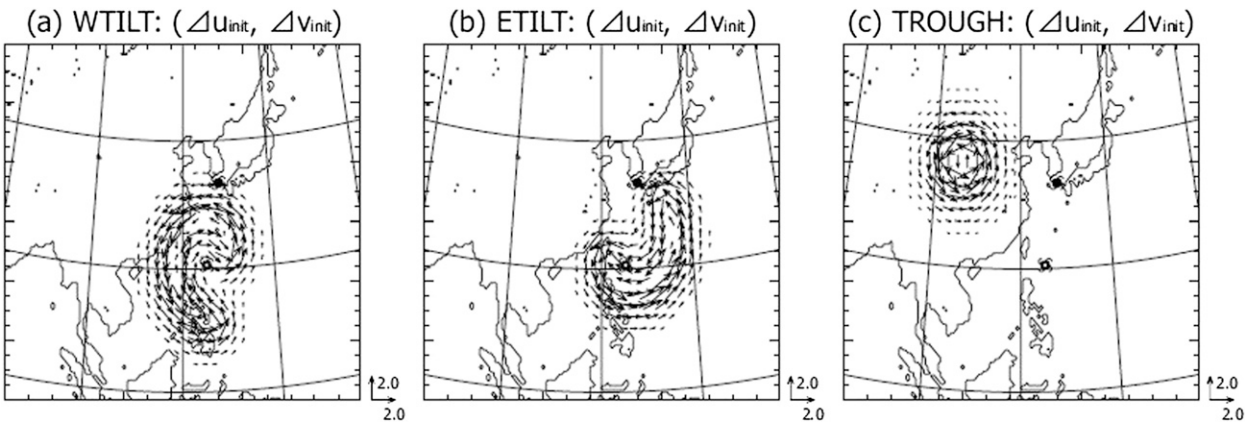

FIG. 7. Horizontal velocity perturbations relative to CTRL in (a) WTILT, (b) ETILT, and (c) TROUGH. Unit vectors for horizontal wind fields ($m\,s^{-1}$) are shown on the rhs of each panel. Vectors that are too small are not plotted. The TC symbol with the center dot is the position of Typhoon Shanshan at the initial time, while the solid one is the ensemble-mean position at the verification time in the CTRL run.

longitude and latitude at 0000 UTC 17 September are 0.422° and 0.384° (a distance of 39 and 43 km), respectively.

b. Ensemble-based sensitivity

Figure 6 shows the sensitivity field of the TC central latitude with respect to the vorticity field at three vertical levels (σ = 0.8445, 0.5060, and 0.2879) for the verification time of 12, 24, and 48 h. The values are horizontally interpolated into the model grid points with a cubic spline. The circles superposed in these figures indicate the *t*-test results. The sensitivity related to the vorticity field is less significant at σ = 0.998 85 and σ = 0.101 than at σ = 0.8445, 0.5060, and 0.2879 (figures not shown). The signals are the strongest at the verification time of 48 h, which reflects the fact that the signals are relevant to the ratio of the change in the TC central latitude at the verification time as a response to the unit initial change. The evolution of the initial perturbation brings about large ensemble-mean changes in the TC central latitude, particularly associated with the swift passage as the TC interacts with midlatitude troughs. Another notable feature is that the major signals are sufficiently far away from the lateral boundary, implying that the regional model is able to reasonably reproduce the TC track, at least within this time scale.

Here, we briefly outline the structure of the sensitivity field. Further investigations on the physical interpretation and comparison of other methods will be presented in Part II. Figure 6 shows that the largest sensitivity near the TC center appears at σ = 0.5060, with values generally larger than those at σ = 0.2879. These are consistent with results from previous sensitivity studies for Shanshan obtained with the ADSSV and SV methods (Wu et al. 2009b; Reynolds et al. 2009), implying that TC motion is more sensitive to changes in the middle troposphere.

For the sensitivity field at the verification time of 12 h, the north–south dipole pattern appears to be centered at the initial TC position. A vertically coherent structure is present from the lower troposphere to the middle troposphere with the largest sensitivity occurring in the latter. This dipole pattern is to some extent relevant to the latitudinal displacement of the vortex. This implies that the appropriate positioning of the vortex is an important element for improving short-term track predictions (Ito et al. 2013). It is notable that the sensitivity signal of meridional velocity in ADSSV (Wu et al. 2007)[3] at the verification time of 12 h exhibits a west–east dipole pattern in contrast to the signals in TyPOS. Physical interpretation of this difference will also be investigated in Part II.

The sensitivity field exhibits a horizontally tilted pattern centered at the initial TC position with respect to the vorticity field in the middle troposphere. This pattern is typically found in ADSSV-based sensitivity analyses (Wu et al. 2007, 2009b; Chen et al. 2011). It is intriguing that the negative sensitivity signals are well developed from east to southwest relative to the initial TC position with extended verification time, which is consistent with the stronger sensitivity signals for Shanshan obtained from ADSSV (Wu et al. 2009b; Chen et al. 2011). The confidence level is above 99.9%. This feature is also detected in the SV-based sensitivity analysis at the recurvature stage for Shanshan (Reynolds et al. 2009).

[3] To avoid misunderstanding, note that the directions of the vectors in TyPOS and ADSSV have different physical implications.

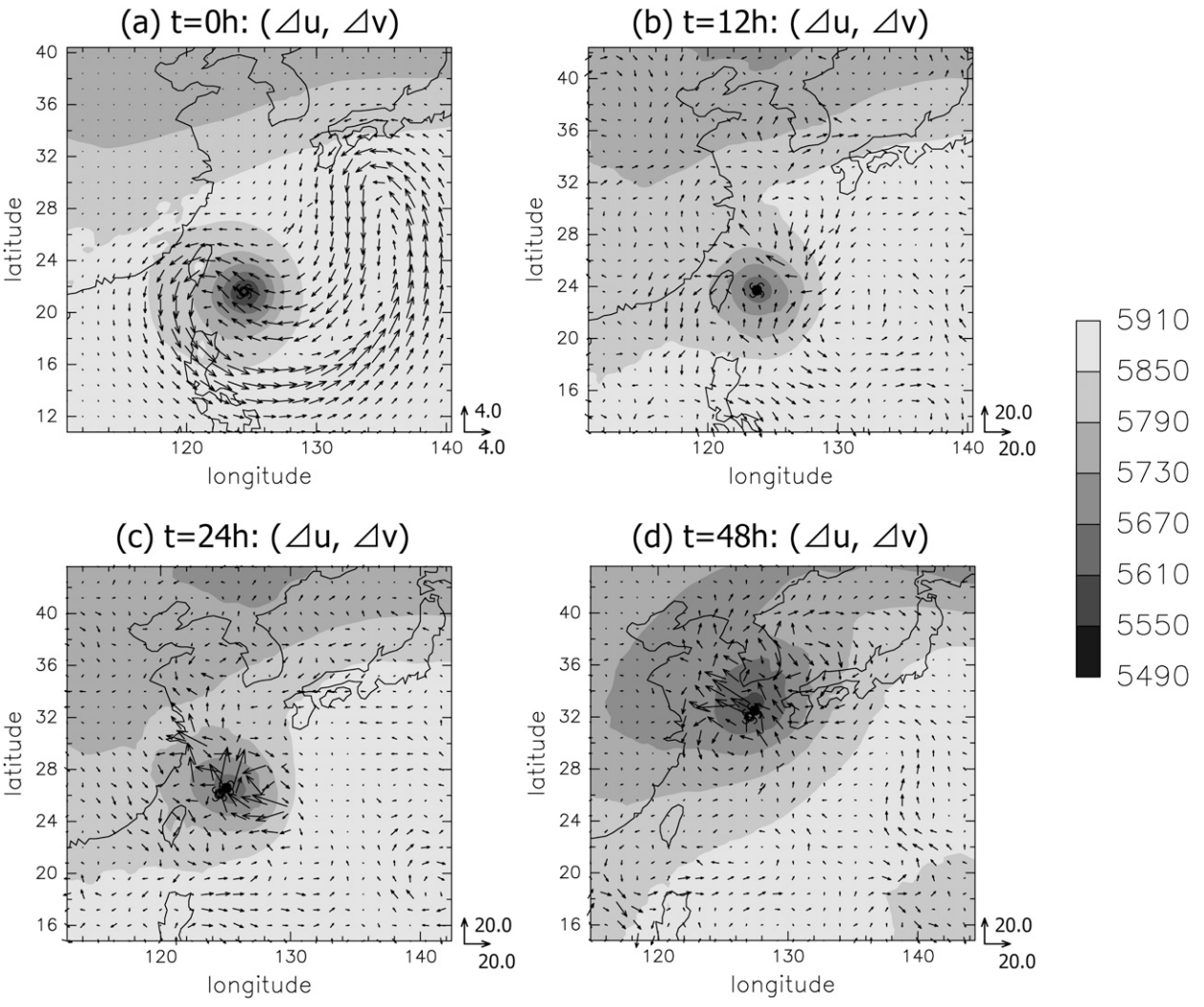

FIG. 8. Time evolution of horizontal velocity perturbations on 500 hPa in ETILT_m001 relative to CTRL_m001 at (a) 0, (b) 12, (c) 24, and (d) 48 h. Unit vectors for horizontal wind fields ($m\,s^{-1}$) are shown on the rhs of each panel. Shading indicates the geopotential height in CTRL_m001. The TC symbol with the dot is the TC position in ETILT_m001, while the solid one indicates that of CTRL_m001.

Besides the horizontally tilted pattern in the middle troposphere, the sensitivity field is elongated northwestward in the upper layer at the verification time of 48 h, presumably because of the strong southeastward wind. This feature is also detected and investigated as a sign of interactions between the TC and midlatitude trough from sensitivity signals of ADSSV (Wu et al. 2009b) and SV (Reynolds et al. 2009). Under close inspection, our signal around the midlatitude trough is not distinct in the middle troposphere in contrast to the ADSSV- and moist SV-based sensitivity signals.

The confidence levels of the sensitivity signals with respect to the divergence field are mostly below 99% in the lower, middle, and upper troposphere (figures not shown). These sensitivity signals are not organized in synoptic scale, suggesting that the vorticity field is more relevant to the TC motion at least in comparison to the divergence field (consistent with results in Wu et al. 2007). As mentioned above, the sensitivity signals obtained from the existing SV- and ADSSV-based methods are fairly consistent with the signals in TyPOS, although some differences are also identified.

c. *Verification experiment*

To ensure that the sensitivity signals obtained from TyPOS are relevant to the motion of Shanshan, additional ensemble experiments are conducted. One hundred members are randomly sampled from 800 members

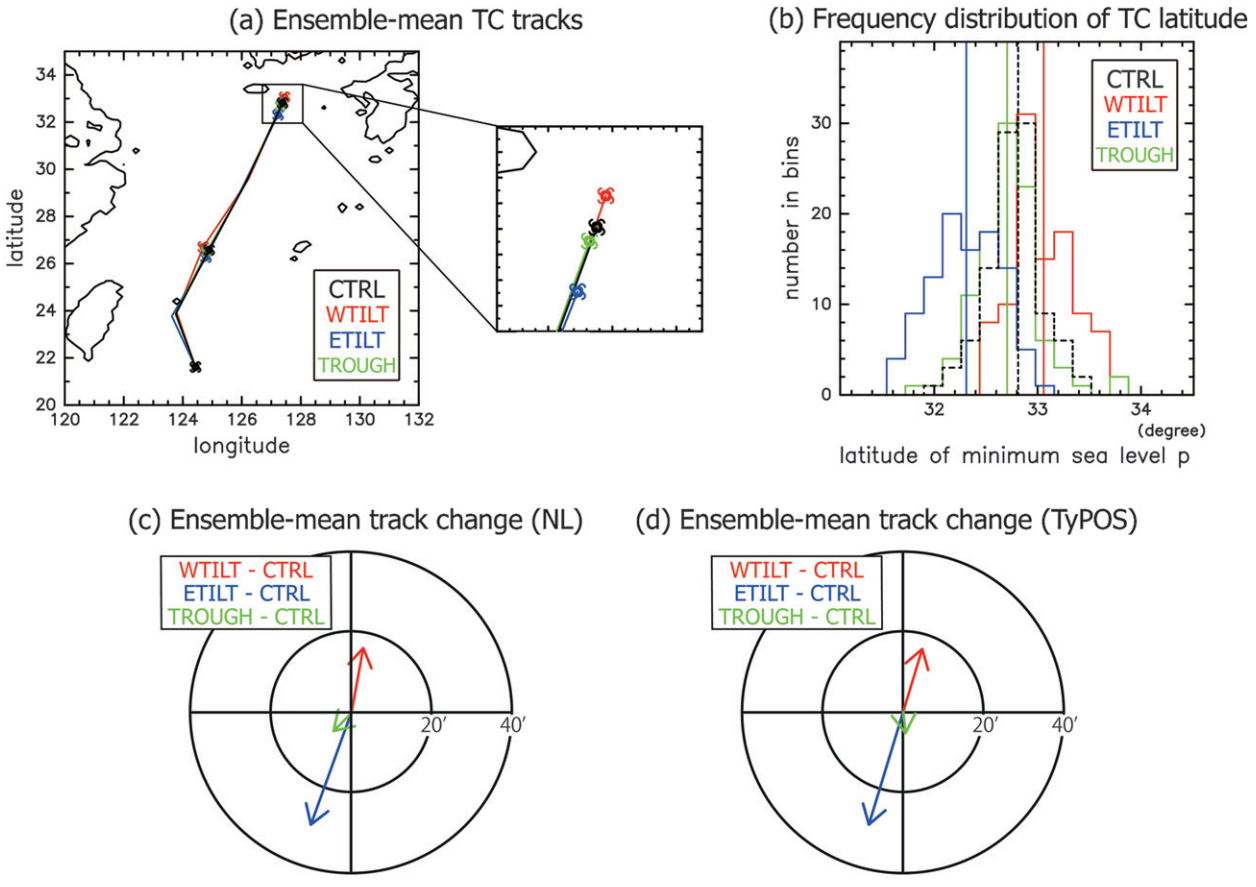

FIG. 9. (a) Ensemble-mean TC track for CTRL (black), WTILT (red), ETILT (blue), and TROUGH (green). (b) Frequency distributions of the TC central latitude at the verification time of 48 h for the results of the CTRL, WTILT, ETILT, and TROUGH runs. Vertical lines denote the ensemble-mean TC central latitude corresponding to the same line color. (c) Ensemble-mean displacement of TC center position (relative to the CTRL run) at the verification time obtained from the nonlinear numerical model run. Horizontal and vertical axes indicate the displacement in longitude and latitude (arc minutes), respectively. (d) As in (c), but for those evaluated by using TyPOS.

used for the sensitivity calculation. This set of 100 ensemble members is referred to as CTRL. We perform ensemble experiments in which three patterns of positive vorticity are added to each initial state of CTRL in the prescribed region. To conduct an ensemble run, the positive vorticity perturbations (without the divergence) are transformed into horizontal velocity perturbations (Δu, Δv), which are the model prognostic variables, via calculations of the streamfunction by solving Poisson's equation. The amplitude of the initial perturbation of u and v is adjusted to the size of standard deviation consistent with the sensitivity analysis.

Here, we investigate the validity of sensitivity field in the middle troposphere with the verification time of 48 h. Two experiments are associated with the strongest sensitivity signals around the initial TC positions and the other experiment is associated with the midlatitude trough in the middle troposphere where differences arise between TyPOS and existing methods. We refer to these three experiments as follows: (i) WTILT is the experiment in which the positive vorticity perturbation is added to the regions consistent with the horizontally tilted pattern west to the initial TC position from $\sigma =$ 0.661 75 to $\sigma = 0.4082$, (ii) ETILT is the same as WTILT but with the horizontally tilted pattern east to the initial TC position, and (iii) TROUGH is the same as WTILT and ETILT but with the perturbation near the midlatitude trough. Figures 7a–c indicate the initial perturbations of additional horizontal wind in ETILT, WTILT, and TROUGH, respectively. Based on the definition of sensitivity and Fig. 6f, we can expect an ensemble-mean northward (southward) displacement relative to CTRL in the WTILT (ETILT) experiment and a smaller displacement in the TROUGH experiment.

According to Eq. (8), the expected ensemble-mean changes ($\Delta\langle \mathrm{LON}\rangle$ and $\Delta\langle \mathrm{LAT}\rangle$) are evaluated as a

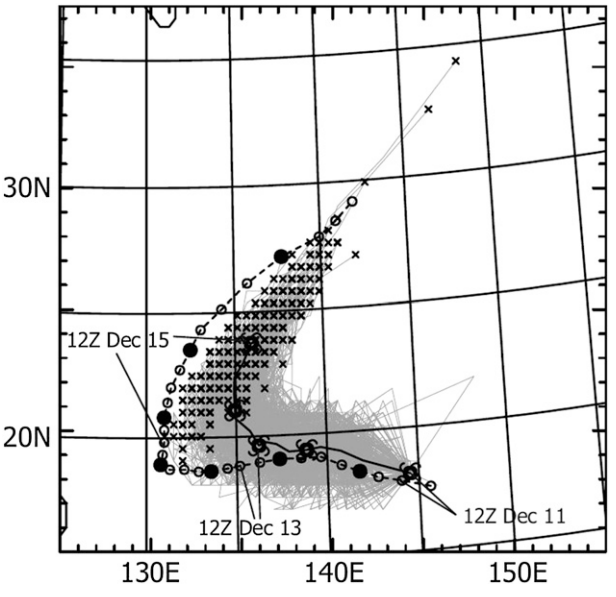

FIG. 10. The TC position from JMA best track for Dolphin plotted over simulated tracks. Open circles indicate the TC positions every 6 h from 0600 UTC 11 Dec, while solid ones indicate the TC positions every 24 h from 0000 UTC 12 Dec. The TC symbols and thick solid lines indicate the ensemble-mean simulated track from 1200 UTC 11 Dec to 1200 UTC 15 Dec. The gray lines correspond to the tracks of each member. The crosses indicate the simulated positions of TC center at 1200 UTC 15 Sep.

response to the additional horizontal wind perturbation at the initial time. As mentioned in section 2b, we multiply the magnitude of perturbations by the sensitivity both of latitude and longitude that are interpolated to the model grid points using a cubic spline:

$$\Delta\langle \mathrm{LON}\rangle \approx \sum_{\mathrm{D1}} \frac{1}{S_{\mathrm{D1}}}(\tilde{\lambda}_u^{\mathrm{LON}}\Delta u + \tilde{\lambda}_v^{\mathrm{LON}}\Delta v) + \sum_{\mathrm{D2}} \frac{1}{S_{\mathrm{D2}}}(\tilde{\lambda}_u^{\mathrm{LON}}\Delta u + \tilde{\lambda}_v^{\mathrm{LON}}\Delta v) \quad \text{and} \tag{9}$$

$$\Delta\langle \mathrm{LAT}\rangle \approx \sum_{\mathrm{D1}} \frac{1}{S_{\mathrm{D1}}}(\tilde{\lambda}_u^{\mathrm{LAT}}\Delta u + \tilde{\lambda}_v^{\mathrm{LAT}}\Delta v) + \sum_{\mathrm{D2}} \frac{1}{S_{\mathrm{D2}}}(\tilde{\lambda}_u^{\mathrm{LAT}}\Delta u + \tilde{\lambda}_v^{\mathrm{LAT}}\Delta v), \tag{10}$$

where the subscripts D1 and D2 represent domain 1 and domain 2, and S_{D1} and S_{D2} are set to constant values of 617.7 and 6273.5, respectively.

d. Results of the verification experiment

Figure 8 shows a typical example of time evolution of horizontal velocity perturbation in a member of the ETILT experiment (ETILT_m001) relative to a corresponding member of the control experiment (CTRL_m001). Perturbations are developed in a broader region within the first 12 h (Fig. 8b). They continue to grow around the TC with maximum values of about 20 m s^{-1} (Figs. 8c,d), appearing to exhibit a cyclonic circulation southwest to the TC position and an anticyclonic circulation northeast at the verification time. This is consistent with the southwestward displacement of the TC in ETILT_m001 relative to that in CTRL_m001.

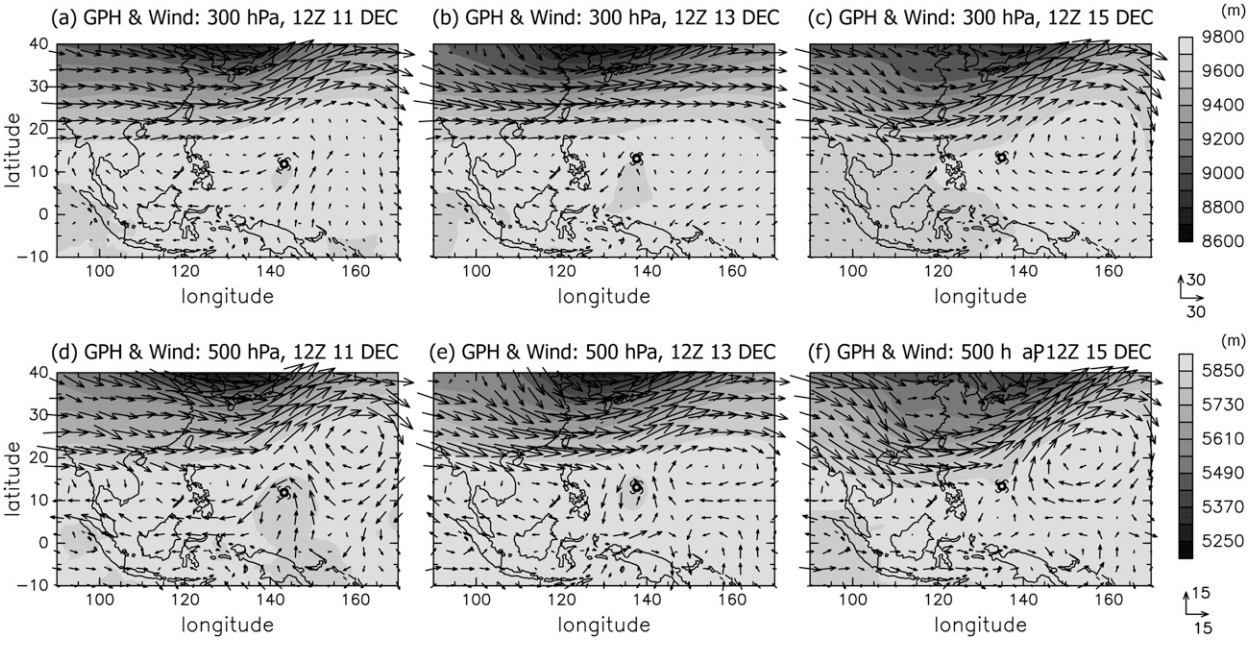

FIG. 11. As in Fig. 5, but for ensemble-mean geopotential height and horizontal wind around Dolphin at (a),(d) 1200 UTC 11 Dec, (b),(e) 1200 UTC 13 Dec, and (c),(f) 1200 UTC 15 Dec.

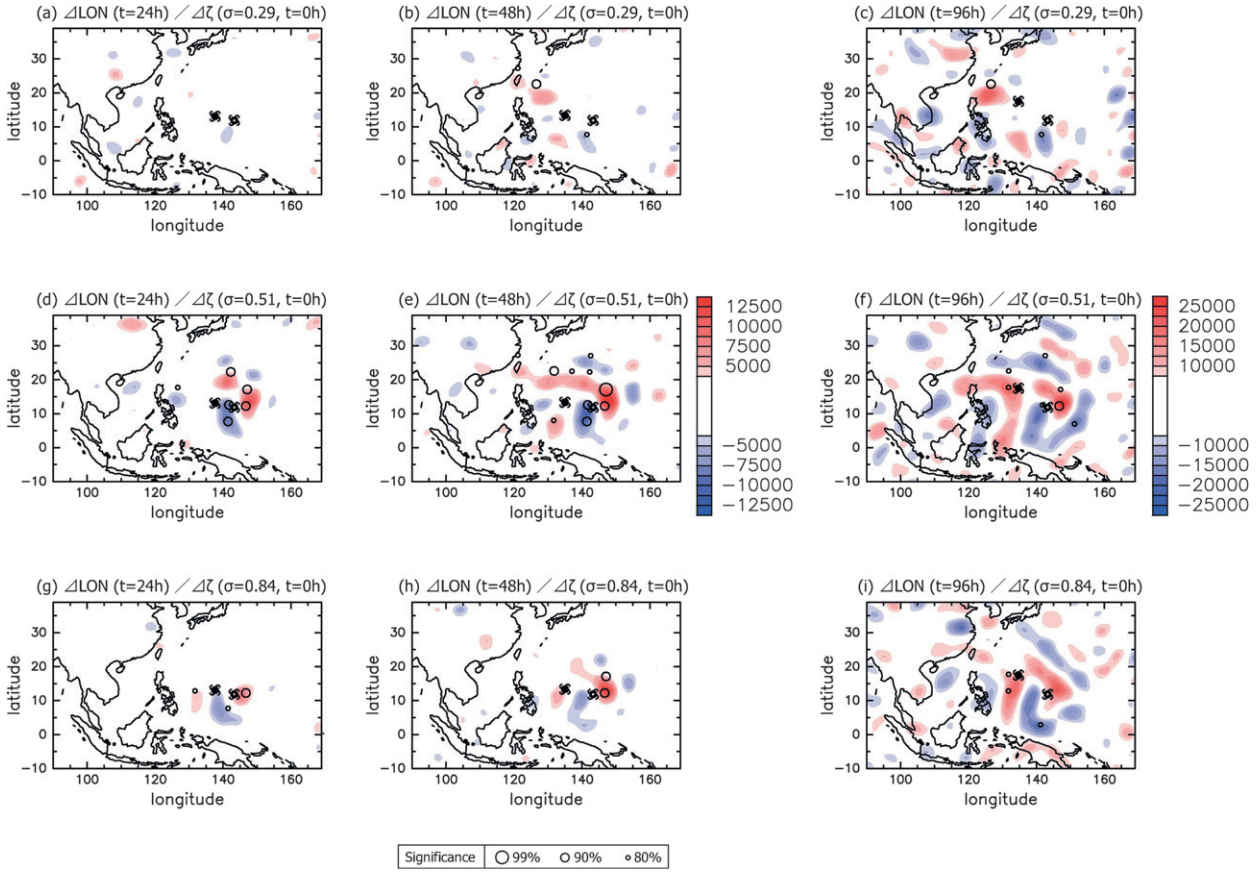

FIG. 12. As in Fig. 6, but for the sensitivity of Dolphin's longitude at the verification time of 24, 48, and 96 h.

Figure 9a shows the ensemble-mean TC positions in different experiments. The members in the WTILT run tend to move northward relative to the CTRL run, while the members in the ETILT run tend to move southward. This finding is consistent with the results of the sensitivity analysis. Ensemble-mean displacement in the TROUGH experiment remains small as expected. It does not necessarily mean that the existing methods overestimate the sensitivity associated with the midlatitude trough in the middle troposphere because the sensitivity is also dependent on the numerical model and the characteristics of initial perturbations. Nevertheless, the results demonstrate that TyPOS accurately reflects the sensitivity of TC position as a response to large-scale initial perturbation for a given ensemble forecast system.

Figure 9b shows the frequency distributions of TC central latitude of the 100 members among different ensemble experiments. It is obvious that the ensemble-mean TC position in WTILT (ETILT) is located to the north (south) of the TC position in CTRL, while the distribution overlaps among different experiments. The current method is shown to be relevant to the changes in probability density function of TC positions.

Figure 9c illustrates the ensemble-mean TC position change relative to CTRL with nonlinear model calculation. The TC displacement estimated from TyPOS quantitatively agrees well with the ensemble-mean displacements in the perturbed experiments (Fig. 9d). We calculate the amplification factor defined as the ratio of total kinetic energy (TKE) of ensemble-mean perturbation integrated over a 1000 km × 1000 km square centered at the TC position at the verification time to that over the entire domain at the initial time. The amplification factors are 1.47 for WTILT, 3.73 for ETILT, and 0.13 for TROUGH at t = 48 h. It is consistent with the largest development of perturbations near Shanshan in the ETILT experiment.

Overall, these features indicate the usefulness of TyPOS. The method can be used to evaluate the expected direction and distance of the vortex displacement as a response to the changes in the initial state and to identify regions that have greater impacts on an ensemble of realizations of the TC forecast position under the probabilistic framework.

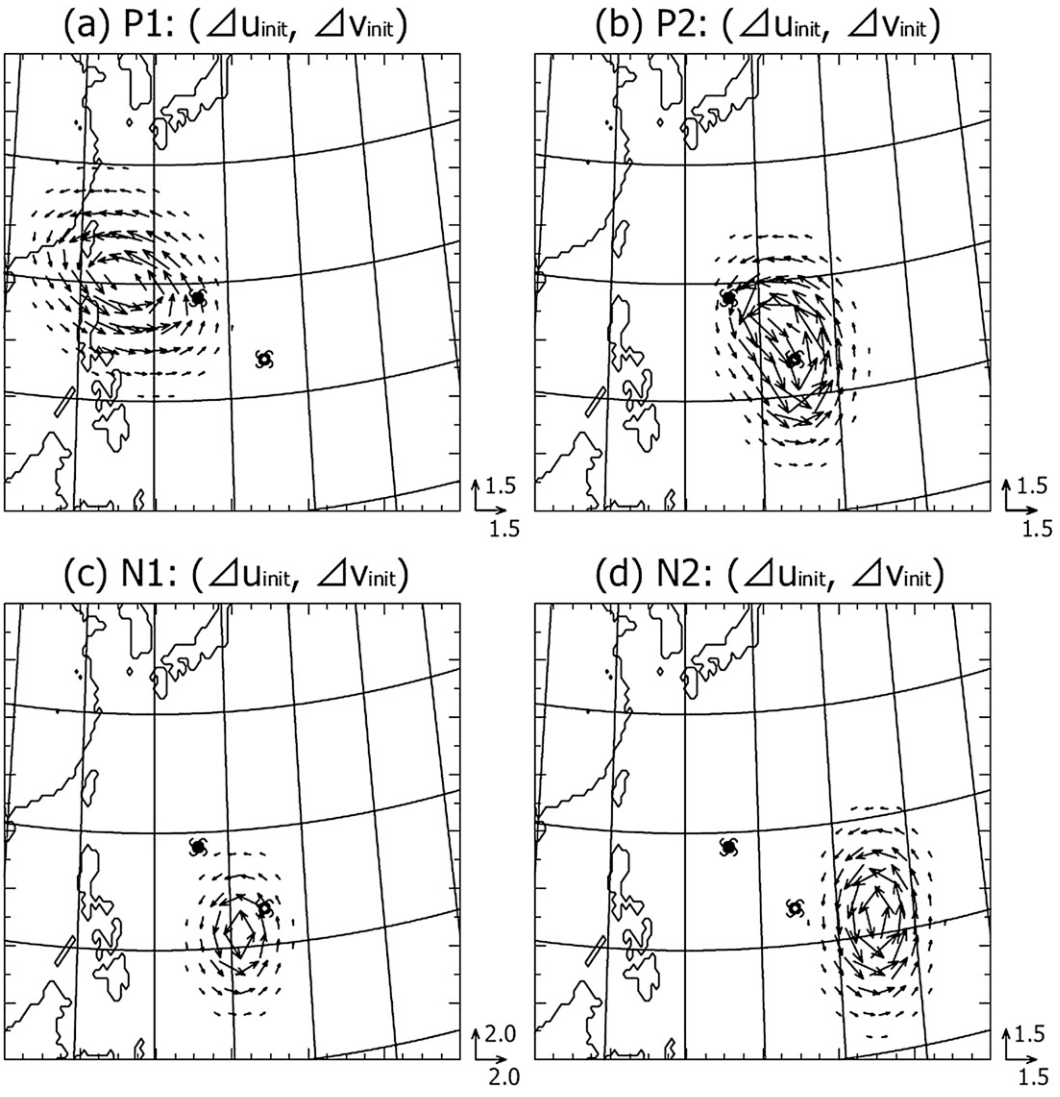

FIG. 13. As in Fig. 7, but for the verification experiment on the sensitivity for Dolphin: (a) P1, (b) P2, (c) N1, and (d) N2.

5. Sensitivity analysis for Dolphin

a. Synopsis and the simulated track

Figure 10 shows the center position of Dolphin in the JMA best track. Dolphin turned into a tropical storm west of the Mariana Islands at 0600 UTC 11 December 2008. After turning sharply to the north around 0000 UTC 15 December, it began to move northeastward on 16 December. The simulated tracks of ensemble members from 1200 UTC 11 December to 1200 UTC 15 December are overlaid with TC symbols in Fig. 10. Simulated tracks generally exhibit early recurvature to the north, while TC position varies greatly at the forecast time of 96 h. Ensemble spreads of the forecasted TC central longitude and latitude at 1200 UTC 15 December are 1.63° and 1.33° (a distance of 166 and 148 km), respectively.

Figure 11 shows that Dolphin was embedded in the easterly wind and was located west of the anticyclonic flow at 1200 UTC 11 December (initial time of the sensitivity analysis). The anticyclonic flow and the midlatitude trough intensified around 14 December and the simulated TCs swiftly moved northeastward toward the direction of flow and the trough.

b. Ensemble-based sensitivity

Figure 12 shows the sensitivity field of the TC central longitude with respect to the vorticity field at three vertical levels (σ = 0.8445, 0.5060, and 0.2879) for the verification time of 24, 48, and 96 h. Values of the sensitivity

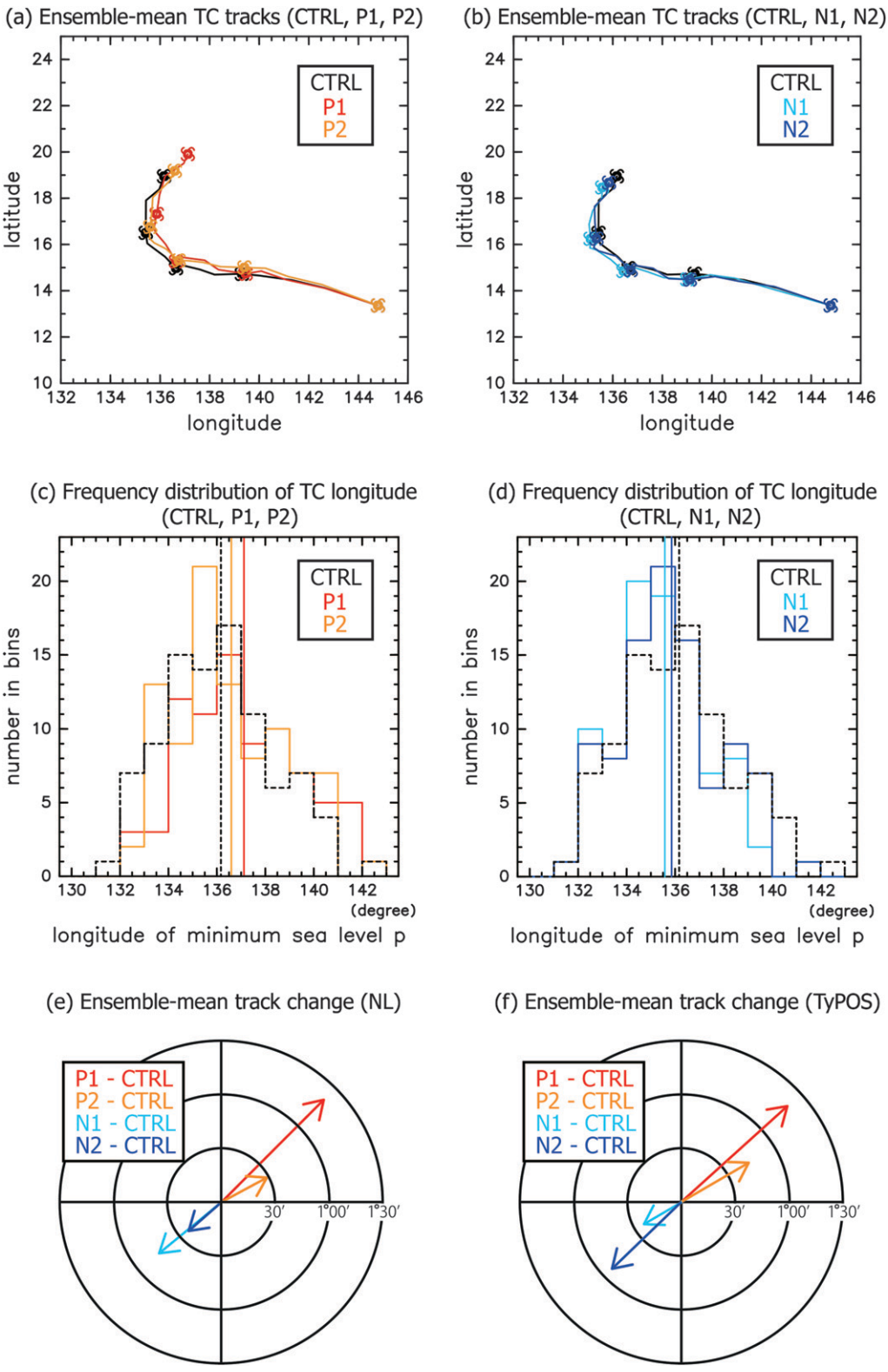

FIG. 14. (a) Ensemble-mean TC tracks of CTRL (black), P1 (red), and P2 (orange). (b) As in (a), but for CTRL, N1 (cyan), and N2 (blue) experiments. (c) Frequency distributions of the TC central longitude at the verification time for CTRL, P1, and P2 runs. (d) As in (c), but for CTRL, N1, and N2 experiments. (e),(f) As in Figs. 9c,d, but for Dolphin at the verification time of 96 h.

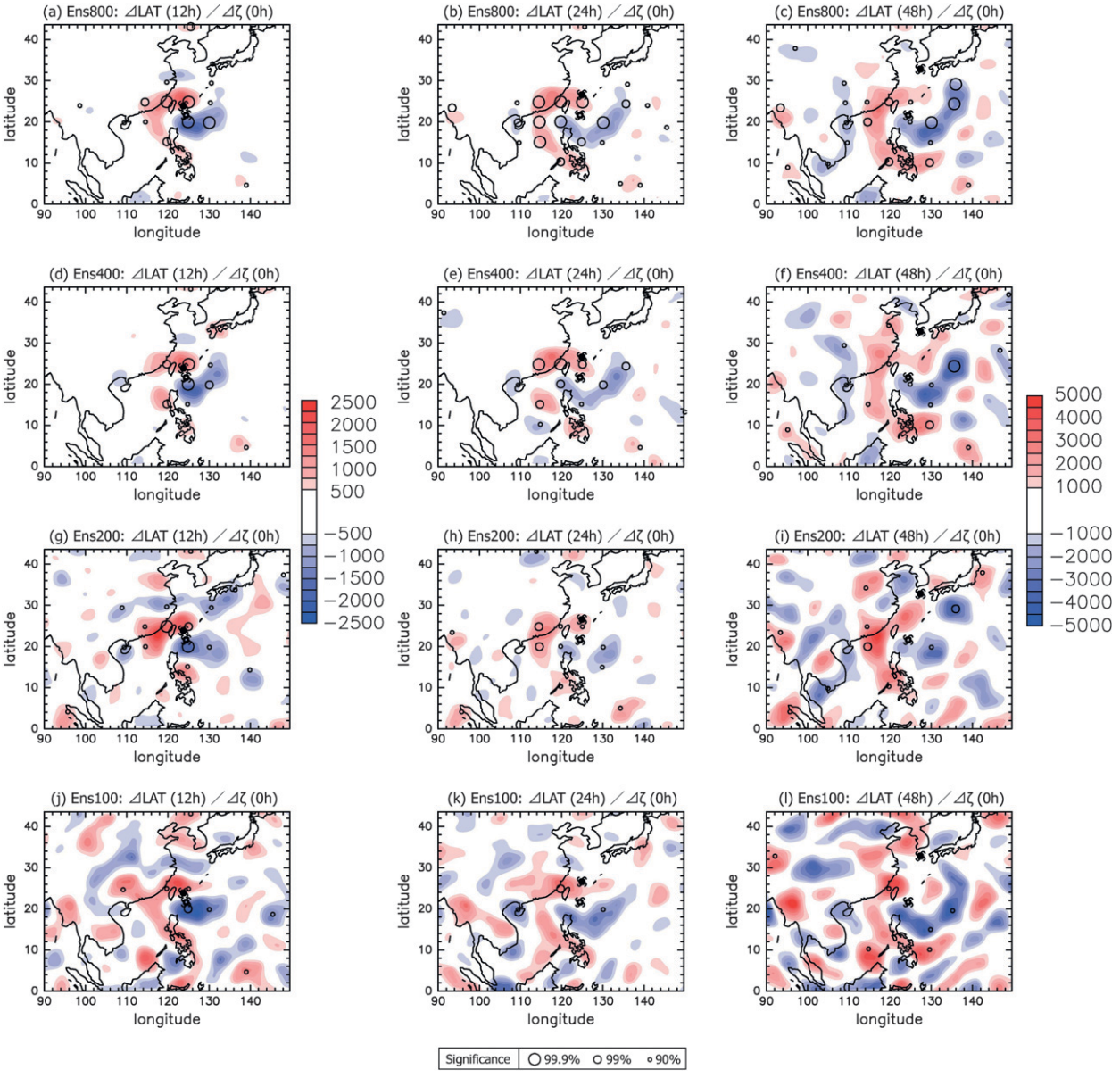

FIG. 15. Sensitivity with respect to the vorticity field at $\sigma = 0.5060$ using (a)–(c) 800, (d)–(f) 400, (g)–(i) 200, and (j)–(l) 100 ensemble members. The metric represents the TC central latitude at (left) 12, (middle) 24, and (right) 48 h.

field at the verification times of 24 and 48 h are large as compared to the sensitivity of the forecasted latitude of Shanshan. This suggests that ensemble-mean TC position change is more sensitive to the initial perturbation. The sensitivity with respect to the vorticity field is less significant at $\sigma = 0.998\,85$ and $\sigma = 0.101$ and the same tendency is observed in the sensitivity with respect to the divergence field as described in section 4 (figures not shown).

The largest sensitivity appears at $\sigma = 0.5060$. The values at $\sigma = 0.8445$ and $\sigma = 0.2879$ are generally smaller than those at $\sigma = 0.5060$ regardless of the verification time. While the confidence level is generally low compared to the case of Shanshan, some sensitivity signals have a confidence level over 90% at the verification time of 96 h.

For the sensitivity field at the verification time of 24 h, the east–west dipole pattern appears to be centered at the initial TC position. The positive sensitivity area extends from the east of the initial position to southern Taiwan in the middle troposphere at the verification time of 48 and 96 h. The significant signals are found around 15°–25°N, 120°–130°E, located at the southern part of the westerly jet, which illustrates the influences of the jet on the TC track.

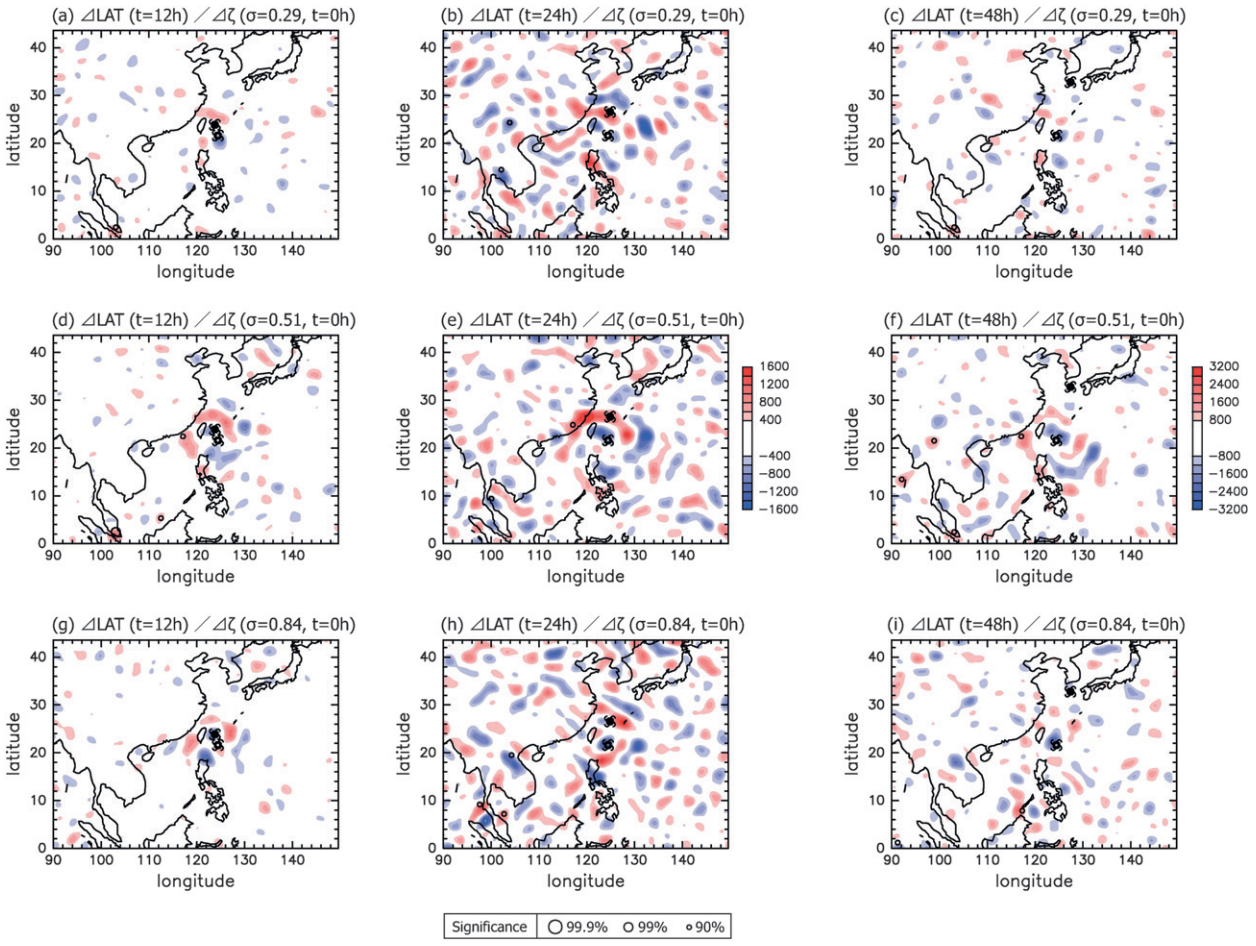

FIG. 16. As in Fig. 6, but for the sensitivity analysis with a reduced grid spacing of 270 km.

c. *Verification experiment*

Four verification experiments are conducted to ensure that the sensitivity signals in the middle troposphere are relevant to the TC position at the verification time of 96 h. Referred to as P1, P2, N1, and N2, the experiments correspond to the significant sensitivity signals around the TC. The procedure of the four experiments is the same as that in section 4c; that is, the positive vorticity perturbations (without divergence) from $\sigma = 0.661\,75$ to $\sigma = 0.4082$ are added to the initial field of the 100-member ensemble run. The initial perturbations of the horizontal wind are shown in Figs. 13a–d. Based on the definition of sensitivity and Fig. 12f, we can expect to observe an ensemble-mean eastward (westward) displacement relative to CTRL in P1 and P2 (N1 and N2) experiments.

The expected ensemble-mean changes ($\Delta\langle\mathrm{LON}\rangle$ and $\Delta\langle\mathrm{LAT}\rangle$) as a response to the constant perturbation in the initial state are evaluated according to the equation below:

$$\Delta\langle\mathrm{LON}\rangle \approx \sum_D \frac{1}{S_D}(\tilde{\lambda}_u^{\mathrm{LON}}\Delta u + \tilde{\lambda}_v^{\mathrm{LON}}\Delta v) \quad \text{and} \tag{11}$$

$$\Delta\langle\mathrm{LAT}\rangle \approx \sum_D \frac{1}{S_D}(\tilde{\lambda}_u^{\mathrm{LAT}}\Delta u + \tilde{\lambda}_v^{\mathrm{LAT}}\Delta v), \tag{12}$$

where the subscript D represents the domain and S_D is set to a constant value of 630.

d. *Results of the verification experiment*

Figures 14a and 14b show ensemble-mean tracks of each experiment. It is clear that ensemble-mean displacement at the verification time is consistent with TyPOS. The TC tends to move eastward in the P1 and P2 experiments relative to CTRL, while the ones in the N1 and N2 runs tend to move westward. These tendencies are connected to earlier (later) recurvature in P1 and P2 (N1 and N2) experiments. Figures 14c and 14d show the frequency distributions of longitude among different ensemble experiments. Although the frequency distributions are

heavily overlapped, the ensemble-mean value is different among the different experiments.

Figure 14e illustrates the ensemble-mean TC position displacement calculated in a nonlinear model. It is qualitatively consistent with the evaluation by using TyPOS (Fig. 14f), with a significant signal only slightly above 80%, indicating a difference from the case of Shanshan that yields a rather quantitative result. Nevertheless, these results show potential of TyPOS for long-term forecast sensitivity analyses. The amplification factors with the verification time of $t = 96$ h are 3.78 for N1, 1.01 for N2, 5.06 for P1, and 0.79 for P2. These values correspond to the large displacement in N1 and P1.

6. Discussion

a. Dependency on ensemble size and resolution

It is important to investigate the dependency of the sensitivity analysis on the number of ensemble members. The sensitivity analysis is conducted based on 400, 200, and 100 ensemble members for the same case (Typhoon Shanshan) described in sections 3 and 4. Figure 15 shows the sensitivity field at $\sigma = 0.5060$ with respect to the vorticity field, superposed with the results of significance t test. The north–south dipole pattern at the verification time of 12 h and the horizontally tilted patterns centered at the initial TC position are found in the sensitivity field with fewer number of ensemble members.

However, some spurious features appear away from the TC center and the confidence level of the signals decreases with a smaller number of ensemble members. One encouraging result is that noise caused by the decreasing number of ensemble members is not detected as significant in most of the cases, although some signals (e.g., 32°N, 92°E in Fig. 15l) indicate a 90% confidence level.

So far, the reduced grid spacing is set to 540 km, which is too coarse to investigate finescale structures. Another sensitivity analysis is performed by halving the horizontal reduced grid spacing to 270 km for Typhoon Shanshan (2006). With the exception of the reduced grid spacing, the settings are the same as in the original one described in sections 3 and 4. Figure 16 shows the sensitivity fields with respect to the vorticity fields. The sensitivity fields are consistent with the findings shown in section 4 in that the horizontally tilted pattern is found near the initial TC position. However, the sensitivity field is contaminated by statistical noise and the signals are seldom considered significant.

This suggests that TyPOS starting from large-scale perturbations can serve as a promising method for both targeted observation operations and research purposes, given the large number of ensemble members. In TyPOS, an additional assumption is introduced to fully determine n elements of the sensitivity field from m realizations as explained in section 2a. Thus, the sensitivity field is not likely to reflect the relationship between input physical variables and the output scalar as the number of degrees of freedom increases. Recent developments in large parallel computer systems with thousands of processors make it possible to obtain sensitivity fields from a very large number of nonlinear forward model runs with full physics (Martin and Xue 2006). However, without enough computational resources, this method provides less reliable features or is merely useful for capturing some features in the further reduced-dimension space. In terms of the operational ensemble forecast, it would be possible to use a basis function corresponding to the fast-developing mode as discussed below or to shrink the domain size of initial perturbations along with the reduction of ensemble size.

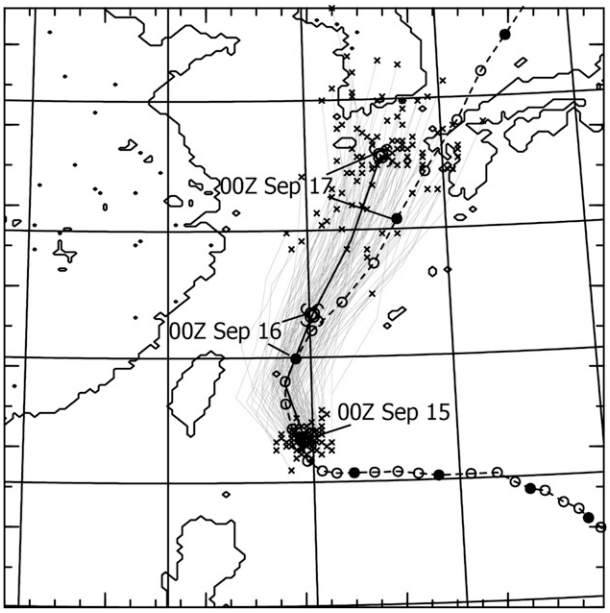

FIG. 17. As in Fig. 4, except that the ensemble simulations are initialized from EnKF-based perturbations.

b. The use of EnKF-based perturbations

So far, large-scale random initial perturbations are used to illustrate the feasibility of TyPOS. However, the use of faster developing perturbations may help efficiently capture the sensitivity field with a smaller number of ensemble members. Its importance in practical application prompted us to conduct another sensitivity analysis based on 100 ensemble members initialized from EnKF-based perturbations for Shanshan. The settings are the same as in section 4 except that the sensitivity field is derived from Eqs. (3) and (4) by using

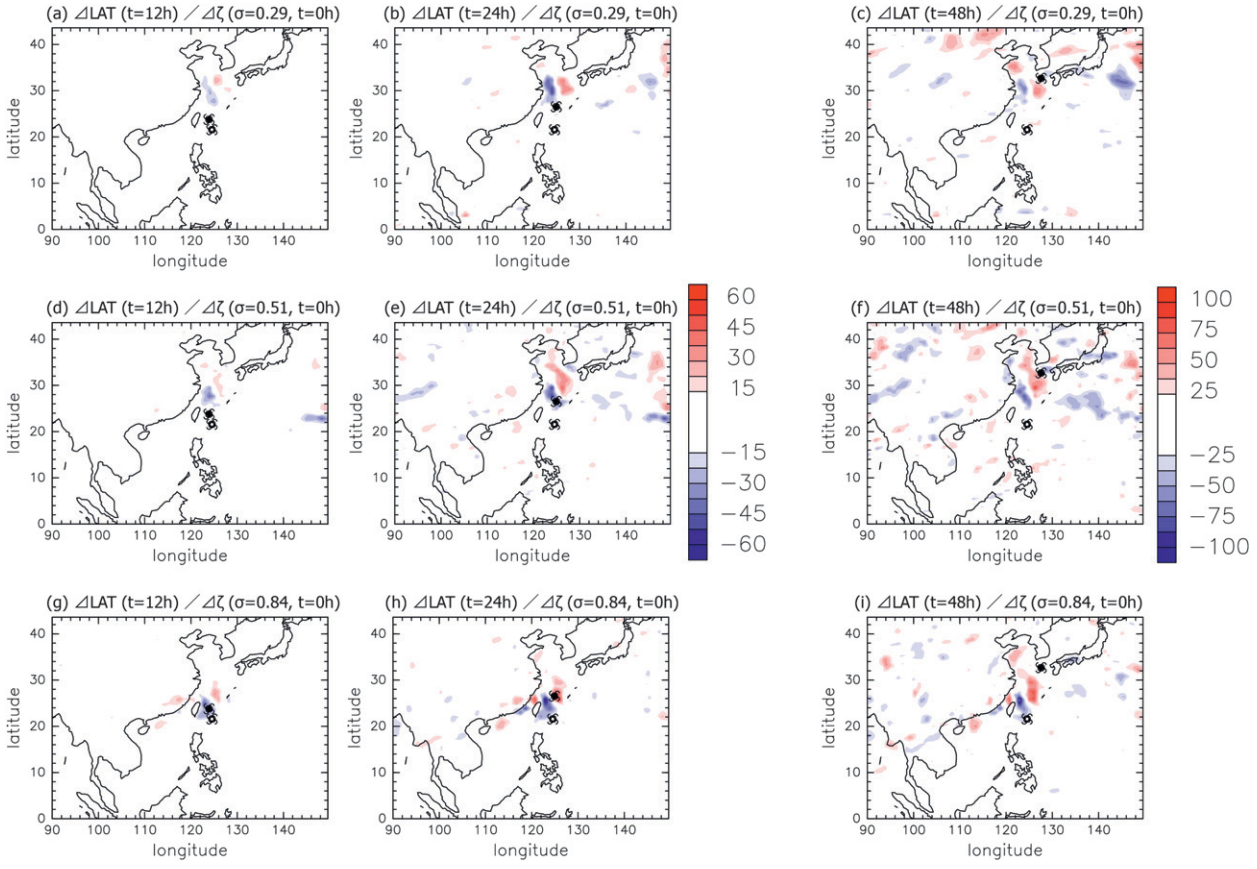

FIG. 18. As in Fig. 6, except that the ensemble simulations are initialized from EnKF-based perturbations.

EnKF-based perturbations instead of large-scale uncorrelated perturbations.

Figure 17 shows the TC forecast tracks initialized from EnKF-based perturbations. Ensemble spreads of the forecasted TC central longitude and latitude at 0000 UTC 17 September are 1.22° and 1.40° (a distance of 114 and 156 km), respectively. They are larger than those in section 4 presumably because of the faster development of perturbations and the larger displacement at the initial time. Figure 18 shows the sensitivity of TC forecast latitude with respect to the vorticity field. The values at $\sigma = 0.8445$ and $\sigma = 0.5060$ are larger than those at $\sigma = 0.2879$. Generally speaking, the sensitivity is relatively strong north of 25°N. In particular, there is a pair pattern in the north of the initial TC position that is inclined to the north with increasing altitude. These sensitivity signals are quite different from those obtained in section 4, likely because of the property of perturbations. Detailed discussion on this topic will be covered in future works.

To verify that these sensitivity signals are relevant to the TC motion, two ensemble experiments are performed as in sections 4c and 5c. Initial vorticity perturbation with the magnitude of $\delta\zeta = \alpha\sigma_\zeta\lambda_\zeta^{\mathrm{LAT}}$ is added in the "POSITIVE" experiment, while the initial vorticity perturbation with the magnitude of $\delta\zeta = \alpha\sigma_\zeta\lambda_\zeta^{\mathrm{LAT}}$ is introduced to the other experiment termed "NEGATIVE." Here, σ_ζ is the ensemble spread of the vorticity at the initial time, and α is set to the constant value of 0.01 so that the maximum change is about the size of the ensemble spread.

Figure 19 shows that the changes of TC positions are consistent with those obtained from the sensitivity field. The vortex displacement as a response to the initial vorticity changes was located in the north-northeast (south southwest) direction as expected, while the distance of displacement is slightly overestimated. It exhibits that 100 EnKF-based perturbations can be utilized to detect the sensitivity of typhoon forecast positions through TyPOS.

7. Concluding remarks

Selection of the forecast metric is one of the critical issues in sensitivity analyses associated with studies of TC motion. In this study, we proposed a typhoon-position-oriented sensitivity analysis (TyPOS) for an ensemble

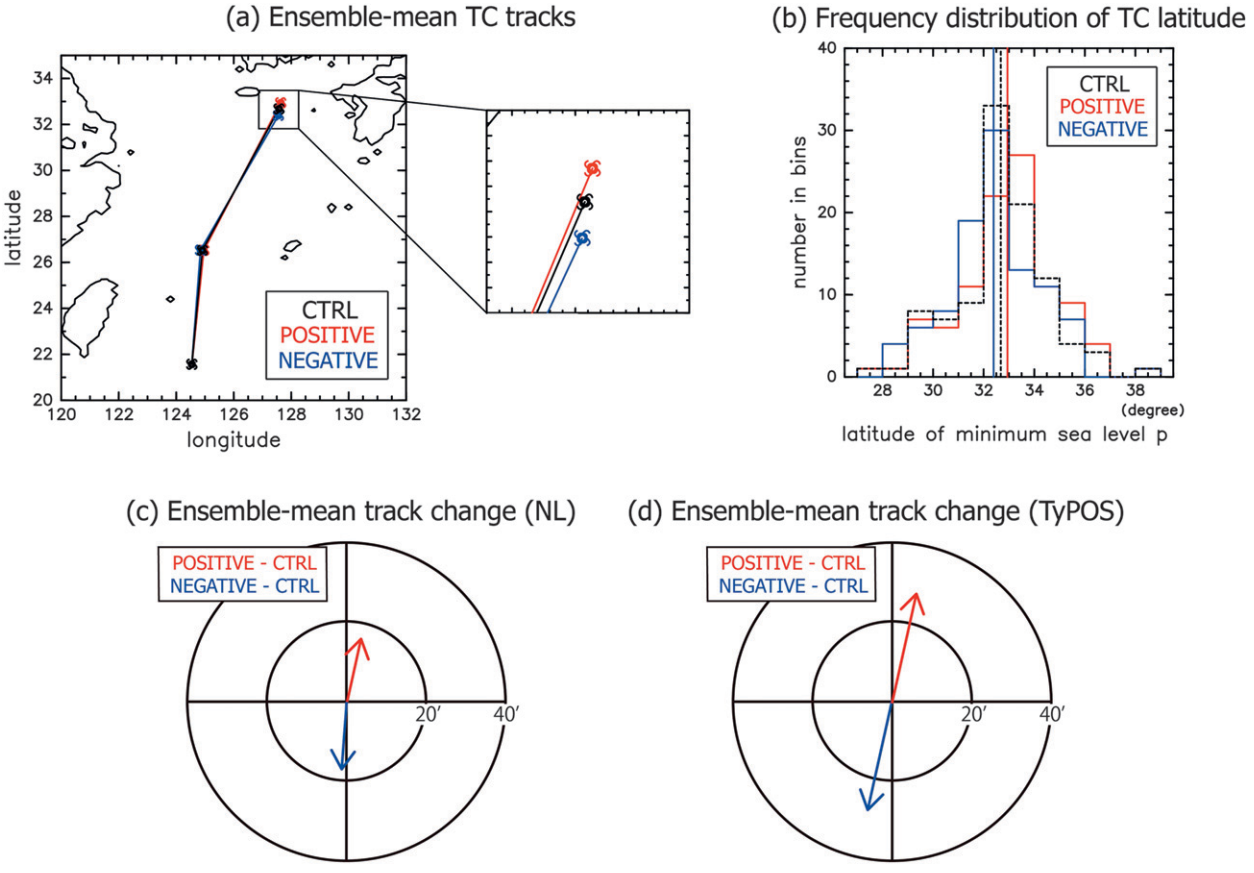

FIG. 19. As in Fig. 9, but for the POSITIVE and NEGATIVE experiments.

forecast system. The sensitivity is interpreted as the slope of the regression line (or its approximation) based on the ensemble simulation between the initial perturbations and the resulted forecast scalar metric representing the TC position.

As a first step, Typhoon Shanshan (2006) and Typhoon Dolphin (2008) are used to demonstrate the applicability of TyPOS as a response to large-scale initial perturbations. The sensitivity field of the TC central latitude with respect to the vorticity field is maximized in the middle troposphere. Interestingly, the sensitivity field is characterized by a dipole pattern and the horizontally tilted patterns centered at the initial TC position. The sensitivity signals related to the vorticity field in the middle troposphere are stronger than those in other altitudes, while the sensitivity related to the divergence field is less significant. This indicates that the sensitivity signals shown by TyPOS are fairly consistent with the signals obtained from existing methods, although there are still a few differences.

The sensitivity signals can be utilized to evaluate the changes in the ensemble-mean TC position as a response to the changes in the initial condition. They are also useful for determining which observations are more likely to objectively contribute to improving ensemble track forecasts. The verification experiments confirm that sensitivity signals in TyPOS reflect the displacement of the TC forecast position even at the verification time of 96 h.

As mentioned above, TyPOS is a useful method to resolve problems in the choice of metrics. However, further improvements are needed because TyPOS is still subject to a variety of uncertainties in specifying initial perturbation magnitudes and patterns. In particular, limitations resulting from the large-scale perturbations would make it difficult to address the finer structure of the sensitivity field. Some noise arises as the number of ensemble members decreases and also with a finer horizontal grid spacing, although the *t*-test results serve as a tool to evaluate whether the acquired signals are reliable or not.

The use of the EnKF-based perturbations may help efficiently capture the sensitivity field with a smaller number of ensemble members and reflect the sophisticated treatment of perturbation development through a data assimilation system. Another sensitivity analysis

based on 100 members initialized from EnKF-based perturbations is conducted for Shanshan. It is encouraging to find that the ensemble-mean displacement of TC forecast position is consistent with that expected by the sensitivity field. However, the sensitivity for EnKF-based perturbations is clearly different from that obtained for large-scale perturbations. Further study is required to explain the factors leading to such a difference.

Other issues to be further investigated include the physical interpretation of the signals, detailed comparison with other methodologies, and applications to real cases in which a bimodal distribution of TC positions is obtained from ensemble runs. Despite these remaining problems, the results shown here are meaningful because a distinctly direct sensitivity analysis method for ensemble TC track forecasts is proposed and verified. This method has potentials to contribute to further reductions of ensemble forecast track errors in connection with targeted observations and to improved understanding of physical processes associated with TC motion.

Acknowledgments. Special thanks to J.-H. Chen, S.-G. Chen, G.-Y. Lien, M. Ueno, Y.-H. Huang, N. Sugiura, and T. Unuma for their useful comments in developing the current system. This work was funded by National Science Council (NSC) Grants 98-2111-M-002-008-MY3 and NSC100-2119-M-002-009-MY3 in Taiwan. The figures were produced by the GFD-DENNOU Library.

REFERENCES

Aberson, S., 2003: Targeted observations to improve operational tropical cyclone track forecast guidance. *Mon. Wea. Rev.,* **131,** 1613–1628.

——, and J. Franklin, 1999: Impact on hurricane track and intensity forecasts of GPS dropwindsonde observations from the first-season flights of the NOAA Gulfstream-IV jet aircraft. *Bull. Amer. Meteor. Soc.,* **80,** 421–427.

Ancell, B., and G. Hakim, 2007: Comparing adjoint- and ensemble-sensitivity analysis with applications to observation targeting. *Mon. Wea. Rev.,* **135,** 4117–4134.

Aonashi, K., and H. Eito, 2011: Displaced ensemble variational assimilation method to incorporate microwave imager brightness temperatures into a cloud-resolving model. *J. Meteor. Soc. Japan,* **89,** 175–194.

Box, G., and M. Muller, 1958: A note on the generation of random normal deviates. *Ann. Math. Stat.,* **29,** 610–611.

Buizza, R., C. Cardinali, G. Kelly, and J.-N. Thépaut, 2007: The value of observations. II: The value of observations located in singular-vector-based target areas. *Quart. J. Roy. Meteor. Soc.,* **133,** 1817–1832.

Chan, J., 2010: Movement of tropical cyclones. *Global Perspectives on Tropical Cyclones: From Science to Mitigation,* J. C. L. Chan and J. D. Kepert, Eds., World Scientific Publishing, 133–148.

Chen, J.-H., M. S. Peng, C. A. Reynolds, and C.-C. Wu, 2009: Interpretation of TC forecast sensitivity from the SV perspective. *J. Atmos. Sci.,* **66,** 3383–3400.

Chen, S.-G., C.-C. Wu, J.-H. Chen, and K.-H. Chou, 2011: Validation and interpretation of adjoint-derived sensitivity steering vector as targeted observation guidance. *Mon. Wea. Rev.,* **139,** 1608–1625.

Chou, K.-H., and C.-C. Wu, 2008: Typhoon initialization in a mesoscale model—Combination of the bogused vortex and the dropwindsonde data in DOTSTAR. *Mon. Wea. Rev.,* **136,** 865–879.

——, ——, P.-H. Lin, S. Aberson, M. Weissmann, F. Harnisch, and T. Nakazawa, 2011: The impact of dropwindsonde observations on typhoon track forecasts in DOTSTAR and T-PARC. *Mon. Wea. Rev.,* **139,** 1728–1743.

Dudhia, J., 1989: Numerical study of convection observed during the winter monsoon experiment using a mesoscale two-dimensional model. *J. Atmos. Sci.,* **46,** 3077–3107.

Elsberry, R., 1995: Tropical cyclone motion. *Global Perspectives on Tropical Cyclones,* J. C. L. Chan and J. D. Kepert, Eds., World Meteorological Organization, 106–197.

——, and P. Harr, 2008: Tropical cyclone structure (TCS08) field experiment science basis, observational platforms, and strategy. *Asia-Pac. J. Atmos. Sci.,* **44,** 209–231.

Gombos, D., and J. A. Hansen, 2008: Potential vorticity regression and its relationship to dynamical piecewise inversion. *Mon. Wea. Rev.,* **136,** 2668–2682.

——, R. Hoffman, and J. Hansen, 2012: Ensemble statistics for diagnosing dynamics: Tropical cyclone track forecast sensitivities revealed by ensemble regression. *Mon. Wea. Rev.,* **140,** 2647–2669.

Grell, G., and D. Devenyi, 2002: A generalized approach to parameterizing convection combining ensemble and data assimilation techniques. *Geophys. Res. Lett.,* **29,** 311, doi:10.1029/2002GL015311.

Hong, S.-Y., and J.-O. Lim, 2006: The WRF single-moment 6-class microphysics scheme (WSM6). *J. Korean Meteor. Soc,* **42,** 129–151.

——, J. Dudhia, and S. Chen, 2004: A revised approach to ice microphysical processes for the bulk parameterization of clouds and precipitation. *Mon. Wea. Rev.,* **132,** 103–120.

——, Y. Noh, and J. Dudhia, 2006: A new vertical diffusion package with an explicit treatment of entrainment processes. *Mon. Wea. Rev.,* **134,** 2318–2341.

Huang, Y.-H., M. Montgomery, and C.-C. Wu, 2012: Concentric eyewall formation in Typhoon Sinlaku (2008). Part II: Axisymmetric dynamical processes. *J. Atmos. Sci.,* **69,** 662–674.

Ito, K., T. Kawabata, T. Kato, Y. Honda, Y. Ishikawa, and T. Awaji, 2013: Simultaneous optimization of air-sea exchange coefficients and initial conditions near a tropical cyclone with JNoVA. *J. Meteor. Soc. Japan,* in press.

Japan Meteorological Agency, cited 2009: Annual report on the activities of the RSMC Tokyo-Typhoon Center 2008. [Available online at http://www.jma.go.jp/jma/jma-eng/jma-center/rsmc-hp-pub-eg/AnnualReport/2008/Text/Text2008.pdf.]

——, cited 2010: Annual report on the activities of the RSMC Tokyo-Typhoon Center 2009. [Available online at http://www.jma.go.jp/jma/jma-eng/jma-center/rsmc-hp-pub-eg/AnnualReport/2009/Text/Text2009.pdf.]

Kim, H.-M., and B.-J. Jung, 2009: Singular vector structure and evolution of a recurving tropical cyclone. *Mon. Wea. Rev.,* **137,** 505–524.

——, S.-M. Kim, and B.-J. Jung, 2011: Real-time adaptive observation guidance using singular vectors for Typhoon Jangmi (200815) in T-PARC 2008. *Wea. Forecasting,* **26,** 634–649.

Kleist, D. T., and M. C. Morgan, 2005: Interpretation of the structure and evolution of adjoint-derived forecast sensitivity gradients. *Mon. Wea. Rev.,* **133,** 466–484.

Komaromi, W., S. Majumdar, and E. Rappin, 2011: Diagnosing initial condition sensitivity of Typhoon Sinlaku (2008) and Hurricane Ike (2008). *Mon. Wea. Rev.,* **139,** 3224–3242.

Liu, C., Q. Xiao, and B. Wang, 2008: An ensemble-based four-dimensional variational data assimilation scheme. Part I: Technical formulation and preliminary test. *Mon. Wea. Rev.,* **136,** 3363–3373.

Majumdar, S., S. Aberson, C. Bishop, R. Buizza, M. Peng, and C. Reynolds, 2006: A comparison of adaptive observing guidance for Atlantic tropical cyclones. *Mon. Wea. Rev.,* **134,** 2354–2372.

——, S. Chen, and C. Wu, 2011: Characteristics of ensemble transform Kalman filter adaptive sampling guidance for tropical cyclones. *Quart. J. Roy. Meteor. Soc.,* **137,** 503–520.

Martin, W., and M. Xue, 2006: Sensitivity analysis of convection of the 24 May 2002 IHOP case using very large ensembles. *Mon. Wea. Rev.,* **134,** 192–207.

Matsumoto, M., and T. Nishimura, 1998: Mersenne twister: A 623-dimensionally equidistributed uniform pseudo-random number generator. *ACM Trans. Model. Comput. Simul.,* **8,** 3–30.

Meng, Z., and F. Zhang, 2007: Tests of an ensemble Kalman filter for mesoscale and regional-scale data assimilation. Part II: Imperfect model experiments. *Mon. Wea. Rev.,* **135,** 1403–1423.

——, and ——, 2008a: Tests of an ensemble Kalman filter for mesoscale and regional-scale data assimilation. Part III: Comparison with 3DVAR in a real-data case study. *Mon. Wea. Rev.,* **136,** 522–540.

——, and ——, 2008b: Tests of an ensemble Kalman filter for mesoscale and regional-scale data assimilation. Part IV: Comparison with 3DVAR in a month-long experiment. *Mon. Wea. Rev.,* **136,** 3671–3682.

Menke, W., 1989: *Geophysical Data Analysis: Discrete Inverse Theory.* 2nd ed. International Geophysics Series, Vol. 45, Academic Press, 289 pp.

Mlawer, E., S. Taubman, P. Brown, M. Iacono, and S. Clough, 1997: Radiative transfer for inhomogeneous atmospheres: RRTM, a validated correlated-*k* model for the longwave. *J. Geophys. Res.,* **102** (D14), 16 663–16 682, doi:10.1029/97JD00237.

Mu, M., F. Zhou, and H. Wang, 2009: A method for identifying the sensitive areas in targeted observations for tropical cyclone prediction: Conditional nonlinear optimal perturbation. *Mon. Wea. Rev.,* **137,** 1623–1639.

National Hurricane Center, cited 2012: National Hurricane Center forecast verification. [Available online at http://www.nhc.noaa.gov/verification/.]

Peng, M., and C. Reynolds, 2006: Sensitivity of tropical cyclone forecasts as revealed by singular vectors. *J. Atmos. Sci.,* **63,** 2508–2528.

——, R. Maue, C. Reynolds, and R. Langland, 2007: Hurricanes Ivan, Jeanne, Karl (2004) and mid-latitude trough interactions. *Meteor. Atmos. Phys.,* **97,** 221–237.

Reynolds, C. A., M. S. Peng, S. J. Majumdar, S. D. Aberson, C. H. Bishop, and R. Buizza, 2007: Interpretation of adaptive observing guidance for Atlantic tropical cyclones. *Mon. Wea. Rev.,* **135,** 4006–4029.

——, ——, and J.-H. Chen, 2009: Recurving tropical cyclones: Singular vector sensitivity and downstream impacts. *Mon. Wea. Rev.,* **137,** 1320–1337.

Sugiura, N., 2010: A research on data assimilation methods towards the estimation and the prediction of ocean variabilities on seasonal, interannual, and decadal timescales (in Japanese). Ph.D. dissertation, Kyoto University, 144 pp.

Torn, R., and G. Hakim, 2008: Ensemble-based sensitivity analysis. *Mon. Wea. Rev.,* **136,** 663–677.

——, and ——, 2009: Initial condition sensitivity of western Pacific extratropical transitions determined using ensemble-based sensitivity analysis. *Mon. Wea. Rev.,* **137,** 3388–3406.

Weissmann, M., and Coauthors, 2011: The influence of assimilating dropsonde data on typhoon track and midlatitude forecasts. *Mon. Wea. Rev.,* **139,** 908–920.

Wilks, D., 2005: *Statistical Methods in the Atmospheric Sciences.* 2nd ed. Academic Press, 648 pp.

Wu, C.-C., and K. Emanuel, 1993: Interaction of a baroclinic vortex with background shear: Application to hurricane movement. *J. Atmos. Sci.,* **50,** 62–76.

——, and Y.-H. Kuo, 1999: Typhoons affecting Taiwan: Current understanding and future challenges. *Bull. Amer. Meteor. Soc.,* **80,** 67–80.

——, and Coauthors, 2005: Dropwindsonde observations for typhoon surveillance near the Taiwan Region (DOTSTAR): An overview. *Bull. Amer. Meteor. Soc.,* **86,** 787–790.

——, J.-H. Chen, P.-H. Lin, and K.-H. Chou, 2007: Targeted observations of tropical cyclone movement based on the adjoint-derived sensitivity steering vector. *J. Atmos. Sci.,* **64,** 2611–2626.

——, and Coauthors, 2009a: Intercomparison of targeted observation guidance for tropical cyclones in the northwestern Pacific. *Mon. Wea. Rev.,* **137,** 2471–2492.

——, S.-G. Chen, J.-H. Chen, K.-H. Chou, and P.-H. Lin, 2009b: Interaction of Typhoon Shanshan (2006) with the midlatitude trough from both adjoint-derived sensitivity steering vector and potential vorticity perspectives. *Mon. Wea. Rev.,* **137,** 852–862.

——, G.-Y. Lien, J.-H. Chen, and F. Zhang, 2010: Assimilation of tropical cyclone track and structure based on the ensemble Kalman filter (EnKF). *J. Atmos. Sci.,* **67,** 3806–3822.

——, S.-G. Chen, C.-C. Yang, P.-H. Lin, and S. Aberson, 2012a: Potential vorticity diagnosis of the factors affecting the track of Typhoon Sinlaku (2008) and the impact from dropwindsonde data during T-PARC. *Mon. Wea. Rev.,* **140,** 2670–2688.

——, Y.-H. Huang, and G.-Y. Lien, 2012b: Concentric eyewall formation in Typhoon Sinlaku (2008). Part I: Assimilation of T-PARC data based on the ensemble Kalman filter (EnKF). *Mon. Wea. Rev.,* **140,** 506–527.

Yamaguchi, M., T. Iriguchi, T. Nakazawa, and C.-C. Wu, 2009: An observing system experiment for Typhoon Conson (2004) using a singular vector method and DOTSTAR data. *Mon. Wea. Rev.,* **137,** 2801–2816.

——, T. Nakazawa, and K. Aonashi, 2012: Tropical cyclone track forecasts using JMA model with ECMWF and JMA initial conditions. *Geophys. Res. Lett.,* **39,** L09801, doi:10.1029/2012GL051473.

Yoden, S., 2007: Atmospheric predictability. *J. Meteor. Soc. Japan,* **85,** 77–102.